Received: 15 November 2022 | Revised: 6 March 2023 | Accepted: 5 April 2023

DOI: 10.1111/bph.16090

THEMED ISSUE ARTICLE

NanoBiT- and NanoBiT/BRET-based assays allow the analysis of binding kinetics of Wnt-3a to endogenous Frizzled 7 in a colorectal cancer model

Lukas Grätz[1] | Joanna J. Sajkowska-Kozielewicz[2,3] | Janine Wesslowski[4] | Julia Kinsolving[1] | Lloyd J. Bridge[5] | Katja Petzold[2,6] | Gary Davidson[4] | Gunnar Schulte[1] | Paweł Kozielewicz[1]

[1]Department of Physiology and Pharmacology, Karolinska Institute, Stockholm, Sweden

[2]Department of Medical Biochemistry and Biophysics, Karolinska Institute, Stockholm, Sweden

[3]Department of Organic and Physical Chemistry, Faculty of Pharmacy, Medical University of Warsaw, Warsaw, Poland

[4]Institute of Biological and Chemical Systems-Functional Molecular Systems, Karlsruhe Institute of Technology, Karlsruhe, Germany

[5]Department of Computer Science and Creative Technologies, University of the West England, Bristol, UK

[6]Department of Medical Biochemistry and Microbiology, Uppsala University, Uppsala, Sweden

Correspondence
Gunnar Schulte, Department of Physiology and Pharmacology, Karolinska Institute, Stockholm, Sweden.
Email: gunnar.schulte@ki.se

Funding information
Cancerfonden, Grant/Award Numbers: CAN2018/715, 20 0264P, 20 1102 PjF; Deutsche Forschungsgemeinschaft, Grant/Award Numbers: 504098926, 331351713-SFB 1324; Knut och Alice Wallenbergs Stiftelse, Grant/Award Number: 2016.0087; Novo Nordisk Fonden, Grant/Award Numbers: NNF22OC0078104, NNF21OC00700, NNF20OC0063168; Stiftelsen Lars Hiertas Minne, Grant/Award Numbers: FO2020-0304, FO2021-0127; Vetenskapsrådet, Grant/Award Number: 2019-01190

Background and Purpose: Wnt binding to Frizzleds (FZD) is a crucial step that leads to the initiation of signalling cascades governing multiple processes during embryonic development, stem cell regulation and adult tissue homeostasis. Recent efforts have enabled us to shed light on Wnt–FZD pharmacology using overexpressed HEK293 cells. However, assessing ligand binding at endogenous receptor expression levels is important due to differential binding behaviour in a native environment. Here, we study FZD paralogue, FZD_7, and analyse its interactions with Wnt-3a in live CRISPR-Cas9-edited SW480 cells typifying colorectal cancer.

Experimental Approach: SW480 cells were CRISPR-Cas9-edited to insert a HiBiT tag on the N-terminus of FZD_7, preserving the native signal peptide. These cells were used to study eGFP-Wnt-3a association with endogenous and overexpressed HiBiT-FZD_7 using NanoBiT/bioluminescence resonance energy transfer (BRET) and NanoBiT to measure ligand binding and receptor internalization.

Key Results: With this new assay the binding of eGFP-Wnt-3a to endogenous HiBiT-FZD_7 was compared with overexpressed receptors. Receptor overexpression results in increased membrane dynamics, leading to an apparent decrease in binding on-rate and consequently in higher, up to 10 times, calculated K_d. Thus, measurements of binding affinities to FZD_7 obtained in overexpressed cells are suboptimal compared with the measurements from endogenously expressing cells.

Conclusions and Implications: Binding affinity measurements in the overexpressing cells fail to replicate ligand binding affinities assessed in a (patho)physiologically relevant context where receptor expression is lower. Therefore, future studies on Wnt–FZD_7 binding should be performed using receptors expressed under endogenous promotion.

KEYWORDS
binding affinity shift, CRISPR-Cas9, FZD_7, NanoBiT/BRET binding, SW480 cells, Wnt

Abbreviations: BRET, bioluminescence resonance energy transfer; CRD, cysteine-rich domain; DKK, Dickkopf; FZD, Frizzled; GPCR, G protein-coupled receptor; HDR, homology-directed repair; LRPs, low-density lipoprotein-receptor-related-protein; SMO, smoothened; Wnt, Wingless/Int-1.

1 | INTRODUCTION

The **10 Frizzleds (FZD_{1-10})** and **smoothened (SMO)** are G protein-coupled receptors (GPCRs), which form Class F of the GPCR superfamily (Foord et al., 2005; Schulte, 2010). While endogenous sterols bind SMO, the 19 different **Wingless/Int-1 (Wnt)** lipoglycoproteins are the main macromolecular ligands of FZDs (Deshpande et al., 2019; Schulte, 2010). Wnt–FZD interactions, which are the sole focus of this work, occur between the protein ligand and the extracellular cysteine-rich domain (CRD) of the receptor (Dijksterhuis et al., 2015; Janda et al., 2012; Schulte & Kozielewicz, 2019; Willert & Nusse, 2012). In addition to FZDs, Wnts also associate with other Wnt receptors, for example, from the lipoprotein-receptor-related-protein family (LRPs) (Davidson, 2021). The binding of Wnts to receptors initiates **β-catenin**-dependent or β-catenin-independent signalling, which regulates multiple processes during embryonic development, stem cell regulation and adult tissue homeostasis (Gordon & Nusse, 2006; Kozielewicz, Turku, & Schulte, 2020). Furthermore, aberrant Wnt signalling is associated with tumorigenesis and other pathologies (Burgy & Konigshoff, 2018; Jung & Park, 2020). Along these lines, the last 30 years of research have provided substantial knowledge about Wnt-induced signalling in healthy and pathophysiological conditions, but we have only recently started to understand the mechanistic and pharmacological details of Wnt–FZD interactions (Bhanot et al., 1996; Jung & Park, 2020; Kozielewicz et al., 2021; Kozielewicz, Turku, & Schulte, 2020; Nusse & Clevers, 2017; Schulte & Wright, 2018; Wesslowski et al., 2020). As such, Wnt–FZD binding has been studied using *in silico* calculations, biochemical and biophysical assays (Agostino et al., 2017; Agostino & Pohl, 2019; Dijksterhuis et al., 2015; Hsieh et al., 1999; Kozielewicz et al., 2021; Sato et al., 2010; Swain et al., 2005; Wesslowski et al., 2020; Wu & Nusse, 2002). Moreover, other studies have provided insight into Wnt-induced CRD dynamics (Kowalski-Jahn et al., 2021) and Wnt-induced conformational changes in the receptor core (Kozielewicz, Turku, Bowin, et al., 2020; Schihada et al., 2020; Wright et al., 2018), using fluorescence-, fluorescence resonance energy transfer (FRET)- and bioluminescence resonance energy transfer (BRET)-based assays applied to live HEK293 cells. These analyses, however, were based on overexpressed receptors in HEK293 cells, an approach that may fail to accurately simulate physiologically relevant conditions (Gibson et al., 2013; Mori et al., 2020). Indeed, recent work on low-density lipoprotein receptor-related protein 6 (LRP6) has demonstrated that the association of **Dickkopf-1 (DKK1)** to LRP6 shows a higher affinity for endogenous receptor levels than for overexpressed receptors (Eckert et al., 2020). As it stands, there have been no studies on Wnt binding to an endogenously expressed mammalian, full-length FZD with paralogue resolution and in a pharmacologically sound manner.

To overcome the limitations of overexpression, endogenous proteins can be tagged using genome editing with CRISPR-Cas9 (Hsu et al., 2014). This technology has been employed with success in a number of studies designed to understand the biology of GPCRs (Soave et al., 2021) and on the co-receptor for Wnt/β-catenin signalling, LRP6 (Eckert et al., 2020). Moreover, several studies have reported on NanoBRET ligand binding to endogenous Class A GPCRs, mostly in HEK293 cells (Goulding et al., 2021; Soave et al., 2020; White et al., 2017; White et al., 2019; White et al., 2020; White et al., 2021). Here, as a continuation of our NanoBRET studies on ligand binding to Class F GPCRs (Kozielewicz et al., 2021; Kozielewicz, Bowin, Turku, & Schulte, 2020; Wesslowski et al., 2020), we assessed the binding of functionally validated, fluorescent Wnt—eGFP-tagged mouse **Wnt-3a** (Takada et al., 2018; Wesslowski et al., 2020) to endogenous **FZD_7** in SW480 cells typifying human colorectal cancer, aiming to utilize a more relevant cell model. Similar to our recent study on overexpressed FZDs in HEK293 cells (Kozielewicz et al., 2021), we have employed BRET binding assays based on the NanoBiT system (NanoBiT/BRET binding). Here, receptors are N-terminally tagged with the 11-amino-acid HiBiT peptide and only the subsequent addition of an 18-kDa complementary and cell-impermeable LgBiT protein allows the formation of a catalytically active luciferase (Dixon et al., 2016). In the presence of a fluorescent ligand, this setup enables selective analysis of ligand binding to cell surface receptors in living cells. As such, this assay can be viewed as an optimal tool to study the association between FZDs and their macromolecular ligands, Wnts.

Here, we establish pharmacological parameters of Wnt binding to full-length FZD expressed under control of its endogenous promotor. We focus on 1 of 10 FZD paralogues, FZD_7. We have selected FZD_7 as a model receptor because of its (patho)physiological relevance as recently implied by structural studies (Xu et al., 2021) and drug

What is already known?

- eGFP-Wnt-3a binding to overexpressed FZD_7 in HEK293 cells was previously studied with NanoBiT/BRET binding.
- FZD_7 is a proposed target for cancer treatment.

What does this study add?

- The defined affinity of eGFP-Wnt-3a to endogenously expressed FZD_7 in the low nanomolar range.
- HiBiT-FZD_7 overexpression leads up to 10-fold decrease in binding on-rates compared with endogenously expressed receptors.

What is the clinical significance?

- This study contributes to a better understanding of Wnt-3a–FZD_7 binding kinetics.
- NanoBiT/BRET assay using endogenously receptors is the future for drug discovery involving Class F GPCRs.

development campaigns to identify anti-cancer treatments (Do et al., 2022). Among several cancers in which FZD_7 plays a role, its link to the growth and invasion of colorectal cancer cells has gained considerable attention in the literature (Flanagan et al., 2019; Tran et al., 2021; Ueno et al., 2008; Vincan et al., 2005). In previous studies, FZD_7 biology was investigated using primary cells and patient-derived immortalized cell lines, such as the SW480 colorectal cell model, which were also used in this study (Ueno et al., 2008; Vincan et al., 2007).

Employing the NanoBiT/BRET binding setup in SW480 cells, we detect higher affinity binding (low nanomolar range) of eGFP-Wnt-3a to endogenous HiBiT-FZD_7 compared with its binding to overexpressed HiBiT-FZD_7. As a complement, we demonstrate that measurements of eGFP-Wnt-3a interactions with overexpressed receptors are confounded by altered receptor internalization and enhanced membrane turnover. Additionally, using the NanoBiT approach, we were able to estimate the number of FZD_7 molecules present at the plasma membrane of genome-edited SW480 cells. The presented ligand binding study therefore expands the current knowledge on Wnt-3a/FZD_7 pharmacology and provides a suitable, robust and sought after assay system for compound screening and validation during the development of FZD_7-targeting drugs.

2 | METHODS

2.1 | Cell culture

HiBiT-FZD_7 SW480 (generated in this study), parental SW480 (ATCC) and ΔFZD_{1-10} HEK293T cells were cultured in Dulbecco's modified Eagle's medium (DMEM) supplemented with 10% foetal bovine serum (FBS), 1% penicillin/streptomycin and 1% L-glutamine in a humidified CO_2 incubator at 37°C. The absence of mycoplasma contamination was routinely confirmed by polymerase chain reaction (PCR) using 5′-GGCGAATGGGTGAGTAACACG-3′ and 5′-CGGATAACGCTTGCGACTATG-3′ primers detecting 16S ribosomal RNA of mycoplasma in the media after 2–3 days of cell exposure.

2.2 | CRISPR-Cas9 genome editing

SW480 cells expressing genome-edited FZD_7 with an N-terminal HiBiT tag were generated by CRISPR-Cas9-mediated homology-directed repair (HDR). The sgRNA (5-TCCGTGGTA**CGG**CTGCGCCC-3′; '-' strand. The protospacer adjacent motif [PAM] sequence in bold) used for Cas9 targeting of the N-terminal region of FZD_7 (National Center for Biotechnology Information [NCBI] Reference Sequence: NM_003507.2) was designed with Alt-R™ CRISPR HDR Design Tool and synthesized by Integrated DNA Technologies (IDT). The HDR template (5′-GTGCTGGCGCTGCTGGGCGCACTGTCCGCGGGCGCCGGGGCGGTGAGCGGCTGGCGGCTGTTCAAGAAGATTAGCCAGCCGTACCACGGAGAGAAGGGCATCTCCGTGCCGGACC-3′) containing the native FZD_7 signal peptide (predicted with https://www.ebi.ac.uk/Tools/pfa/phobius/) and the HiBiT tag was designed with Alt-R™ CRISPR HDR Design Tool and synthesized by IDT. The addition of silent mutations was not needed for this design because the HDR mutation sufficiently disrupts the guide sequence. SW480 cells at 4×10^5 cells·ml^{-1} were transfected in suspension using Lipofectamine CRISPRMAX with Plus reagent using the following ratio: [Cas9]:[HDR template]:[sgRNA] = 10 nM:3.0 nM:10 nM and 1 μM of Alt-R HDR enhancer V2 and seeded in a total volume of 150 μl per well in a 96-well plate. The cells were cultured for 24 h in antibiotic-free medium with 10% FBS. Subsequently, two consecutive runs of serial dilutions were performed to obtain single cell (clonal) cultures in wells of a 96-well plate. Following a sufficient growth of the cells (approximately 10 weeks), genomic DNA was isolated using the NaOH/Tris–HCl method and, independently, mRNA was isolated with an mRNA Isolation Kit according to the manufacturer's instructions. mRNA was then used to transcribe cDNA with SuperScript IV reverse transcriptase and random primers (Thermo Fisher Scientific). To amplify the region encompassing the genome-edited sequence, the following pair of PCR primers was used: 5′-ACCCAGGCTGACGAGTTTTG-3′ and 5′-TAGGGCGCGGTAGGGTAG-3′; predicted product size = 829 bp. The final product size was determined using a Bioanalyzer (Agilent 2100, DNA 1000 Assay). The specific PCR products were validated with Sanger sequencing (Eurofins GATC) using the forward primer 5′-ACCCAGGCTGACGAGTTTTG-3′. To visually compare FZD_7 mRNA expression in SW480 and HiBiT-FZD_7 SW480 cells, cDNA was obtained as above and subjected to end-point PCR using different number of cycles (15, 16, 17, 18, 19, 20, 25, 30 and 35). The following primers were used: 5′-TCGACGCTCTTTACCGTTCT-3′ and 5′-GGGCACGGCATAGCTCTT-3′; predicted product size = 743 bp. Additionally, the protein expression of a CRISPR-Cas9-edited FZD_7 with an N-terminal HiBiT tag was assessed with immunoblotting and NanoBiT-emitted luminescence (Figure 1).

2.3 | Preparation of whole-cell lysates

HiBiT-FZD_7 SW480 cells were transiently transfected in suspension using Lipofectamine® 3000 (Thermo Fisher Scientific). A total of $\sim 2 \times 10^6$ cells were transfected in 5 ml with 5000 ng of pcDNA3.1 plasmid DNA (endogenous), 500 ng of HiBiT-FZD_7 plasmid DNA and 4500 ng of pcDNA3.1 plasmid DNA (overexpression) or 5000 ng of HiBiT-FZD_7 plasmid DNA (high overexpression). The cells (5 ml) were seeded and grown to confluency in a 25-cm^2 cell culture flask. Twenty-four hours later, the medium was removed and the cells were washed twice with 5 ml of PBS. The cells were then detached from the flask using PBS and a cell scraper (VWR). The cell suspension in 5 ml of PBS was transferred to a 15-ml conical tube and centrifuged once at 400× g for 5 min at room temperature. The supernatant was aspirated and discarded. Cell pellets were stored at −80°C until required. For homogenization, the cell pellets were resuspended in 1 ml of complete non-phenol red DMEM (HyClone) supplemented with 10 mM of *N*-2-hydroxyethylpiperazine-*N*′-2-ethanesulfonic acid (HEPES) and protease inhibitors. In order to disrupt cell membranes

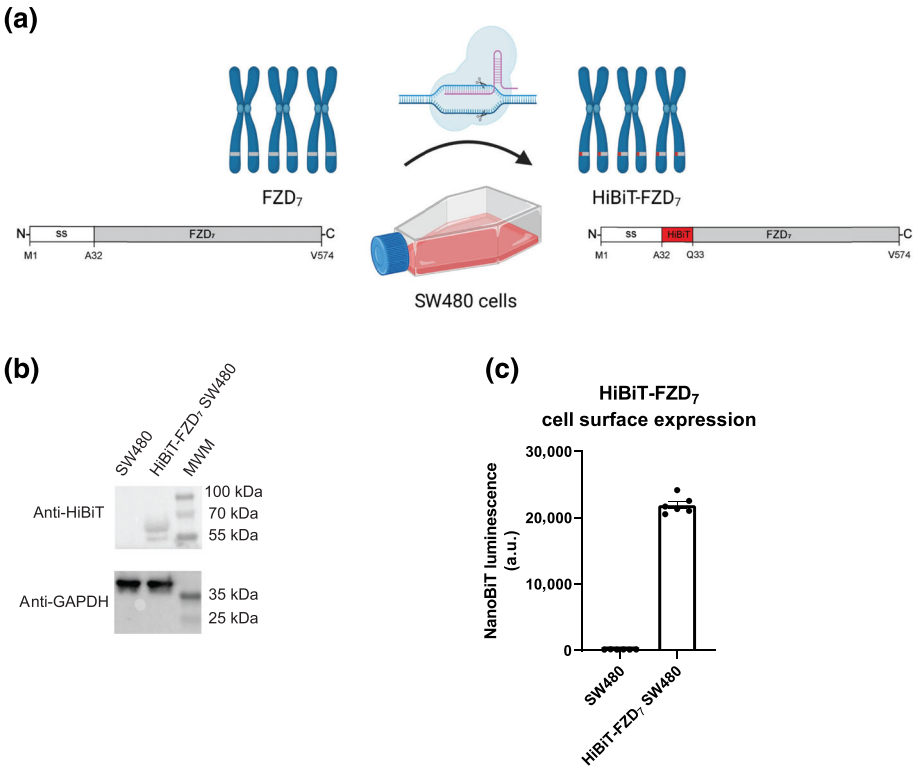

FIGURE 1 Validation of HiBiT-FZD_7 SW480 cells. (a) The scheme depicts the generation of CRISPR-Cas9 genome-edited SW480 cells expressing HiBiT-FZD_7. ss, signal sequence (M1-A32). Generated with BioRender. (b) Validation of cellular expression of endogenous HiBiT-FZD_7 in parental and CRISPR-Cas9 genome-edited SW480 cells. Cell lysates were analysed by immunoblotting using anti-HiBiT antibody and anti-GAPDH served as a loading control. The predicted molecular weight of HiBiT-FZD_7 = 62.0 kDa. Western blot experiments were repeated five times with similar results. MWM, molecular weight marker. (c) Surface expression of HiBiT-FZD_7 was quantified by measuring NanoBiT-emitted luminescence. Raw data are shown from n = 6 individual experiments and are presented as mean ± SEM.

and release cellular contents, homogenization was performed on wet ice by sonication (Sonics Vibra-Cell; 99% power in 3 × 3-s bursts with 3-s pauses). Next, the samples were centrifuged at 400× g for 5 min. Aliquots of the supernatant that contained lysed cells were used immediately in experiments.

2.4 | DNA cloning and mutagenesis

To match the CRISPR-Cas9-edited FZD_7, we removed the GS linker adjacent to the HiBiT tag from a previously published HiBiT-FZD_7 plasmid construct (Kozielewicz et al., 2021) using GeneArt site-directed mutagenesis (Thermo Fisher Scientific) and the following primers: 5′-TTCAAGAAGATTAGCCAGCCGTACCACGGA-3′ and 5′-TCCGTGGTACGGCTGGCTAATCTTCTTGAA-3′. To generate the platelet-derived growth factor receptor TM domain-anchored (Petersen et al., 2017) HiBiT-tagged human FZD_7 CRD (HiBiT-FZD_7-CRD-TM), the FZD_7-CRD sequence (Q33-G200) was amplified from pFastBac-FZD_7 construct (generated in the lab, unpublished) using the following primers: 5′-TCAAGAAGATTAGCGGATCCCAGCCGTAC CACGGAGAGAA-3′ and 3′-GCGAATTCTCCGCTGGAACCGCCAT CTGAGGCCCCCGGGGG-5′. HiBiT-TM was linearized from HiBiT-FZD_5-CRD-TM (generated in the lab, unpublished) with primers 5′-GGTTCCAGCGGAGAATTCGC-3′ and 3′-GGATCCGCTAATCTTCTT-GAAC-5′, and FZD_7-CRD was subcloned in frame into the HiBiT-TM sequence using Gibson cloning. pFastBac backbone was from Thermo Fisher Scientific (#10359016). The constructs were validated by sequencing (Eurofins GATC).

2.5 | Preparation of eGFP-Wnt-3a conditioned media

HEK293F™ suspension cells growing in serum-free Expi293™ expression medium (60 ml, 2.5 × 10^6 cells·ml^{-1}) were cotransfected with 10 μg of pCS2+–eGFP-Wnt-3a together with 50 μg of pCMV-His-Afamin plasmid using ScreenFect® UP-293 (ScreenFect GmbH) according to the manufacturer's instructions. The corresponding control conditioned medium was generated from cells transfected with empty pCS2+ plasmid. Cells were first cleared from the HEK293F™ conditioned medium by centrifugation at 310× g for 10 min and then at 3400× g for 30 min to remove any remaining cellular debris and insoluble material. This 'raw' conditioned medium then was concentrated 5-fold using Vivaspin turbo 15 centrifugal concentrators (30,000-molecular-weight cut-off, Satorius AG, Göttingen, Germany) and exchanged to the desired cell culture medium using Sephadex G-25 PD10 desalting columns (GE Healthcare Bio-Science). The final concentration and integrity of eGFP-Wnt-3a in the conditioned medium were determined using both enzyme-linked immunosorbent assay (ELISA) (GFP ELISA® kit, #ab171581, Abcam) and sodium dodecyl sulfate-polyacrylamide gel electrophoresis (SDS-PAGE)/western blot analysis. From the three eGFP-Wnt-3a batches (eGFP-Wnt-3a Batch 1 final concentration: 21 nM; eGFP-Wnt-3a Batch 2 final concentration: 20 nM; and eGFP-Wnt-3a Batch 3 final concentration: 15.3 nM), Batch 1 was used in optimization experiments and Batches 2 and 3 were used in the experiments presented in this study as described in the figure legends. The eGFP-Wnt-3a concentration was adjusted to 18 nM (for Batch 2) and 13.6 nM (for Batch 3) following

the addition of FBS (to 10% final concentration) and HEPES (to 10 mM of final concentration). Current Wnt purification methods allow only limited Wnt concentration to be obtained from a conditioned medium (Willert, 2008). For the validation of the eGFP-Wnt-3a batches, please see Figure S8.

2.6 | LgBiT/HiBiT calibration curve

One day before the experiment, SW480 cells were seeded at a density of 4×10^4 cells per well (100 µl) onto a poly-D-lysine-coated (Thermo Fisher Scientific) black 96-well cell culture plate with a transparent flat bottom (Greiner BioOne). A white adhesive tape (VWR) was attached to the bottom of the plate before the measurement. On the day of the experiment, cells were washed once with 200 µl of Hanks' balanced salt solution (HBSS) and maintained in 80 µl of complete, non-phenol red DMEM supplemented with 10 mM of HEPES. HiBiT control protein (#N301A, Promega) dilutions were prepared in the same medium and added (10 µl per well). Next, 10 µl of a mix of LgBiT (1:20 dilution; #N2421, Promega) and furimazine (1:10 dilution), prepared in the above-described medium, was added. After an incubation period of 10 min at 37°C (no CO_2), luminescence (460–500 nm, 200 ms of integration time) was recorded using a TECAN Spark microplate reader (TECAN). To estimate the number of FZD_7 molecules on the cell surface, we used the following: the formula from the calibration curve, the Avogadro constant = $6.02214076 \times 10^{23}$ mol^{-1}, average number of cells per well = 72,500 and solution volume in a well = 100 µl.

2.7 | NanoBiT/BRET binding assay

HiBiT-FZD_7 SW480 or SW480 cells were left untransfected or transiently transfected in suspension using Lipofectamine® 2000 (Thermo Fisher Scientific). For overexpression experiments, a total of $\sim 4 \times 10^5$ cells were transfected in 1 ml with 100 ng of HiBiT-FZD_7 plasmid DNA and 900 ng of pcDNA3.1 plasmid DNA (overexpression) or 1000 ng of HiBiT-FZD_7 plasmid DNA (high overexpression). For the HiBiT-FZD_7-CRD-TM experiments, a total of $\sim 4 \times 10^5$ SW480 cells were transfected in 1 ml with 5, 50 or 500 ng of HiBiT-FZD_7-CRD-TM plasmid DNA and 995, 950 or 500 ng of pcDNA3.1 plasmid DNA, respectively. The cells (100 µl) were seeded onto a poly-D-lysine-coated black 96-well cell culture plate with a transparent flat bottom (Greiner BioOne). Before BRET measurements, a white adhesive tape (VWR) was attached to the plate bottom. Twenty-four hours after transfection, the cells nearly doubled (average total cell number in a well = 72,500). They were washed once with 200 µl of HBSS (HyClone). In the kinetic binding experiments, the cells were preincubated with 50 µl of a mix of Nluc substrate endurazine (1:50 dilution; #N2571, Promega) and LgBiT (1:50 dilution; #N2421, Promega) in a complete, non-phenol red DMEM supplemented with 10 mM of HEPES for 90 min at 37°C without CO_2. Subsequently, 50 µl of eGFP-Wnt-3a conditioned medium or control medium supplemented with 10% FBS and 10 mM of HEPES was added and the BRET signal was measured every 87 s for 300 min at 37°C. In the saturation binding experiments with live cells, the cells were incubated with different concentrations of eGFP-Wnt-3a conditioned medium (90 µl) supplemented with 10% FBS and 10 mM of HEPES for 300 min at 37°C (no CO_2). In the saturation binding experiments with whole-cell lysates, 30.5 µl of the lysates was pipetted to respective wells followed by addition of 59.5 µl of different concentrations of eGFP-Wnt-3a conditioned medium. The plate was then incubated for 300 min at 37°C (no CO_2). Next, 10 µl of a mix of furimazine (1:10 dilution; #N2421, Promega) and LgBiT (1:20 dilution; #N2421, Promega) was added. The plates were incubated for another 10 min at 37°C (no CO_2) before starting the BRET measurements. The BRET ratio was defined as the ratio of light emitted by eGFP-Wnt-3a (energy acceptor) and light emitted by HiBiT-FZD_7 (energy donor). Net BRET ratio was defined as BRET ratio (ligand-treated wells)–BRET ratio (vehicle-treated wells). The BRET acceptor (520–560 nm) and BRET donor (460–500 nm) emission signals were recorded with 200 ms of integration time using a TECAN Spark microplate reader (TECAN). Cell surface expression of HiBiT-FZD_7 was assessed by measuring luminescence of vehicle-treated wells (no BRET acceptor) in the NanoBiT/BRET binding assays.

2.8 | Receptor internalization

HiBiT-FZD_7 SW480 cells were left untransfected or transiently transfected in suspension using Lipofectamine® 2000 (Thermo Fisher Scientific). A total of $\sim 4 \times 10^5$ cells were transfected in 1 ml with 100 ng of HiBiT-FZD_7 plasmid DNA and 900 ng of pcDNA3.1 plasmid DNA (overexpression) or 1000 ng of HiBiT-FZD_7 plasmid DNA (high overexpression). The cells (4×10^4 cells in 100 µl) were seeded onto a poly-D-lysine-coated black 96-well cell culture plate with a transparent flat bottom (Greiner BioOne). Twenty-four hours later, the cells were washed once with 200 µl of HBSS (HyClone). Next, 45 µl of a complete, non-phenol red DMEM supplemented with 10 mM of HEPES was added to the wells followed by the addition of 45 µl of 18 nM (9 nM of final concentration) of high-purity recombinant untagged Wnt-3a. The ligand was added every 30 min for 210 min, keeping the cells at 37°C without CO_2. Finally, 10 µl of a mix of furimazine (1:10 dilution; #N2421, Promega) and LgBiT (1:20 dilution; #N2421, Promega) was added 20 min after the last Wnt-3a addition and the plate was incubated for 10 min at 37°C without CO_2. Before the luminescence measurements, the white adhesive tape was attached to the plate bottom. NanoBiT emission (460–500 nm, 200 ms of integration time) was measured using a TECAN Spark microplate reader (TECAN).

2.9 | Immunocytochemistry

SW480 cells or HiBiT-FZD_7 SW480 cells were seeded on poly-D-lysine-coated four-chamber 35-mm dishes (µ-dish 35 mm Quad, Ibidi

#80416). After 1 day, cells were transfected either with 500 ng of pcDNA plasmid DNA (for SW480 and HiBiT-FZD$_7$ SW480 cells) or with HiBiT-FZD$_7$ (no GS linker) plasmid DNA (for the transfected condition) using Lipofectamine 2000 as the transfection reagent according to the manufacturer's instructions. One day after the transfection, the cells were washed once with PBS (with Ca^{2+} and Mg^{2+}, hereafter referred to as 'washing buffer') and fixed using 4% paraformaldehyde in PBS for 10 min at room temperature. The cells were washed three times with the washing buffer and permeabilized with PBS containing 0.25% Triton X-100 (Thermo Fisher Scientific #T8787) for 5 min at room temperature. After three washing steps with washing buffer, samples were blocked using PBTA (PBS with 1% BSA, 0.05% Triton X-100 and 0.02% sodium azide) for 2 h at room temperature and incubated overnight with anti-HiBiT antibody (1 μg·ml^{-1}, Promega, Clone 30E5) in PBTA at 4°C. On the next day, the cells were washed four times with washing buffer, blocked for 30 min at room temperature using PBTA and incubated with an Alexa Fluor 488-conjugated polyclonal goat anti-mouse secondary antibody (IgG, 1 μg·ml^{-1}, Invitrogen #A28175; stock was kept at 4°C), diluted in PBTA, for 2 h at room temperature in the dark. After four washing steps with washing buffer, nuclei were stained using Hoechst 33342 (1 μg·ml^{-1}) for 10 min at room temperature in the dark. Cells were washed once with washing buffer, kept in 0.1% BSA/HBSS and imaged using a Zeiss LSM800 confocal microscope.

2.10 | Immunoblotting

Whole-cell lysates were obtained using Laemmli buffer with 0.5% NP-40 and 5% β-mercaptoethanol. Lysates were sonicated (Soniprep 150, maximal power in 3 × 3-s bursts with 3-s pauses) and analysed on 4–20% Mini-PROTEAN TGX precast polyacrylamide gels (Bio-Rad) together with PageRuler Plus Prestained Protein Ladder (Thermo Fisher Scientific). Proteins were subsequently transferred to polyvinylidene difluoride (PVDF) membranes using the Trans-Blot Turbo system (Bio-Rad). After blocking with 5% non-fat dried milk in Tris/NaCl/Tween20 buffer (TBS-T), membranes were incubated with the following primary antibodies, diluted in blocking buffer: rabbit, monoclonal anti-GAPDH (14C10; 1:2500; Cell Signaling Technology #2118; kept as milk dilution at −20°C and reused tens of times) and mouse, monoclonal anti-HiBiT (1.0 μg·ml^{-1}; Promega clone 30E5; IgG2c with kappa light chain; stock was aliquoted and each aliquot used not more than three times; stored at −20°C), overnight at 4°C. After multiple washing steps with TBS-T, membranes were incubated with horseradish peroxidase-conjugated secondary antibodies, diluted in blocking buffer for 1 h at room temperature (goat anti-rabbit, 1:3000, Invitrogen #31460; or goat anti-mouse, 1:3000, Thermo Fisher Scientific #31430). After multiple washing steps, membranes were incubated for 2 min with Clarity Western ECL Blotting Substrate (Bio-Rad) and proteins were visualized on ChemiDoc (Bio-Rad). The uncropped blots can be found in Figure S9. The immuno-related procedures used comply with the recommendations made by the *British Journal of Pharmacology* (Alexander et al., 2018).

2.11 | Data and statistical analysis

All data presented in this study come from at least five individual experiments (biological replicates) with each individual experiment performed typically in duplicates (technical replicates) for each tested concentration/condition, unless otherwise specified in a figure legend. One biological replicate is defined as wells with cells seeded from the same individual cell culture flasks and measured on the same day. Different biological replicates were transfected using separate transfection mixes and treated with separate ligand dilution series. Technical replicates are defined as individual wells with cells from the same biological replicate treated with the same ligand concentration. Treatment conditions and samples were not randomized or blinded during the experiments. However, to ensure unbiased analysis, the data were analysed in GraphPad Prism 8 or GraphPad Prism 9 using the same built-in equations for a given assay paradigm and no data points were excluded from the analysis. Data points on the binding curves represent mean ± SEM. Kinetic binding data were fit using the association model with two or more hot ligand concentrations (https://www.graphpad.com/guides/prism/latest/curve-fitting/reg_association2.htm), one-phase association (https://www.graphpad.com/guides/prism/8/curve-fitting/REG_Exponential_association.htm) or rise-and-fall to steady state (S. R. J. Hoare et al., 2020). Association rate constants k_{on} and dissociation rate constants k_{off} are presented as a best fit k_{on} ± SEM and best fit k_{off} ± SEM, respectively. Dissociation half-time $t_{1/2}$ is calculated as $\ln 2/k_{off}$ ($0.693/k_{off}$). Equilibrium dissociation constant values (K_d) representing ligand binding affinities from kinetic binding studies calculated as k_{off}/k_{on} are presented with errors propagated as described previously (Gratz et al., 2021). Saturation binding data were fit using a one-site specific model (https://www.graphpad.com/guides/prism/latest/curve-fitting/reg_one_site_specific.htm). Equilibrium dissociation constant values (K_d) representing ligand binding affinities from saturation binding studies are reported as a best fit K_d with 95% confidence intervals (95% CIs). Wnt-3a-induced HiBiT-FZD$_7$ internalization data were normalized to the vehicle-treated wells (100%) and fitted to a fall to steady state time course (endogenous HiBiT-FZD$_7$ expression) or fall-and-rise to baseline (HiBiT-FZD$_7$ overexpression and high overexpression) equations (Hoare et al., 2020). HiBiT–LgBiT calibration data were tested for linearity with the Runs test ($P < 0.05$) and analysed using a simple linear regression model (https://www.graphpad.com/guides/prism/latest/curve-fitting/reg_linearreg.htm) with luminescence intensities and HiBiT concentrations both presented on logarithmic scales. Expression data in Figures 5 and S3B were analysed using the same equations. Statistical analysis, if deemed required, was performed on data coming from at least n = 5 individual experiments with $^*P \leq 0.05$ considered significant. Cell surface expression data with more than two datasets in Figures 2b, 6a,c and S4B are presented as mean ± SEM and were analysed for

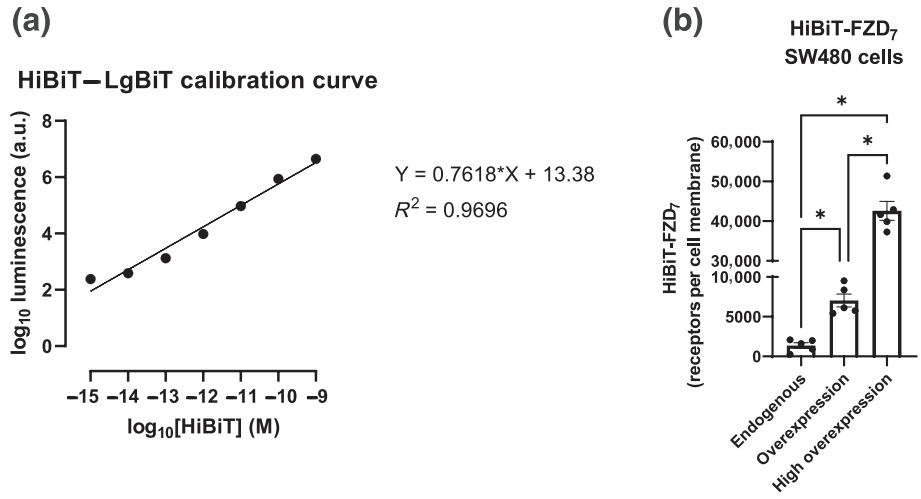

FIGURE 2 Estimation of HiBiT-FZD$_7$ expression on the cell surface of HiBiT-FZD$_7$ SW480 cells. (a) Concentration-dependent effect of purified HiBiT on complemented luminescence following incubation with 1:200 LgBiT and 1:100 furimazine. SW480 cells were plated onto a black transparent-bottom 96-well plate and luminescence was measured in 100 µl of a complete non-phenol red DMEM. Raw data are shown from n = 5 individual experiments and are presented as mean ± SEM; a.u., an arbitrary unit. (b) Surface expression of HiBiT-FZD$_7$ under endogenous, overexpressed and highly overexpressed conditions in the CRISPR-Cas9 genome-edited HiBiT-FZD$_7$ SW480 cells was measured by quantifying NanoBiT-emitted luminescence. The number of membranous receptor molecules estimated using the equation from the panel (a). The average number of cells (72,500 cells per well) was used in the calculations. Data are shown from n = 5 individual experiments and are presented as mean ± SEM. Please refer to Figure S4 for the raw luminescence data. *$P \leq 0.05$.

differences with one-way analysis of variance (ANOVA) followed by the Holm–Šídák post hoc test. Expression data in Figures 6b and S3a were analysed using repeated measures (RM) one-way ANOVA followed by uncorrected Fisher's least significant difference (LSD) post hoc test. Post hoc tests were conducted only if $P < 0.05$ in ANOVA. Expression data with two datasets in Figure 6a are presented as mean ± SEM and were analysed with a Student's unpaired *t*-test. The data and statistical analysis comply with the recommendations of the *British Journal of Pharmacology* on experimental design and analysis in pharmacology (Curtis et al., 2022).

2.12 | Materials

Parental SW480 (ATCC) and ΔFZD$_{1-10}$ HEK293T cells were a kind gift from Benoit Vanhollebeke (Universite Libres de Bruxelles, Belgium). Recombinant untagged high-purity human Wnt-3a (#5036-WNP-010) and recombinant untagged human DKK1 (#5439-DK) were purchased from R&D Systems (Minneapolis, MN, USA). Lipofectamine CRISPRMAX with Plus reagent, penicillin, streptomycin, L-glutamine and Triton X-100 (#T8787) were purchased from Thermo Fisher Scientific (Waltham, MA, USA) plus N-2-hydroxyethylpiperazine-*N*′-2-ethanesulfonic acid (HEPES). The following were obtained from Sigma-Aldrich (St. Louis, MO, USA), Hoechst 33342 (#B2261), foetal bovine serum (FBS), digitonin (#D141), dimethyl sulfoxide (DMSO) and Dulbecco's Modified Eagle's medium (DMEM). Endurazine (#N2571) and LgBiT (#N2421) were obtained from Promega (Madison, WI, USA) along with HiBiT control protein (#N301A). Hanks' balanced salt solution (HBSS) was obtained from HyClone (Logan, UT, USA). All cell culture plastics were from Sarstedt (Numbrecht, Germany) unless otherwise specified, while mRNA Isolation Kit (#11741985001) was obtained from Roche (Rotkreuz, Switzerland). Details of other materials and suppliers are provided in the specific sections.

Recombinant untagged high-purity human Wnt-3a was dissolved at 200 µg·ml^{-1} in sterile 0.1% bovine serum albumin (BSA)/phosphate-buffered saline (PBS) and stored at 4°C. Recombinant untagged human DKK1 was dissolved at 100 µg·ml^{-1} in sterile 0.1% BSA/PBS and stored at 4°C. eGFP-Wnt-3a was prepared as described above. Digitonin was dissolved at 10 mg·ml^{-1} in DMSO, aliquoted and stored at −20°C.

2.13 | Nomenclature of targets and ligands

Key protein targets and ligands in this article are hyperlinked to corresponding entries in the IUPHAR/BPS Guide to PHARMACOLOGY http://www.guidetopharmacology.org and are permanently archived in the Concise Guide to PHARMACOLOGY 2021/22 (Alexander et al., 2021).

3 | RESULTS

3.1 | Genome engineering of SW480 cells

We generated a genome-edited SW480 clonal cell line expressing FZD$_7$ tagged on the N-terminus with the 11-amino-acid HiBiT tag

(hereafter referred to as HiBiT-FZD$_7$ SW480 cells; Figure 1a). Sequencing of the FZD$_7$-specific PCR product amplified from genomic DNA resulted in one distinct sequence, implying that a homozygous clonal line was obtained (Figure S1A,B). These results were confirmed by sequencing of the FZD$_7$-specific PCR product amplified from cDNA reversely transcribed from total cellular mRNA, which also presented itself with a single distinct sequence indicating the sole presence of RNA coding for HiBiT-FZD$_7$ and no untagged FZD$_7$ allele (Figure S1C,D). In agreement with the sequencing data, we could detect full-length HiBiT-FZD$_7$ by immunoblotting (Figure 1b). FZD$_7$ presented itself with two specific bands, which were also present in overexpressed conditions (Figure S2A). Furthermore, we also tested if CRISPR-Cas9 genome editing had an impact on FZD$_7$ gene expression. This exploratory analysis with semi-quantitative PCR suggests that FZD$_7$ mRNA expression is slightly higher in non-modified SW480 cells compared with HiBiT-FZD$_7$ SW480 cells but it is nonetheless within the same range for the two cell lines (Figure S2B). Additionally, we were able to detect bioluminescence following incubation of the live genome-edited SW480 cells with furimazine and the membrane-impermeable LgBiT, indicative of cell-membrane localization of the tagged protein (Figure 1c).

3.2 | Quantification of FZD$_7$ expression in HiBiT-FZD$_7$ SW480 cells

Expression levels of HiBiT-FZD$_7$ molecules at the plasma membrane of live CRISPR-Cas9-edited SW480 cells were estimated using NanoBiT-emitted luminescence and a LgBiT–HiBiT calibration curve. Here, the addition of increasing concentrations of purified HiBiT in the presence of fixed working dilutions of LgBiT and furimazine led to a linear increase in luminescence presented on a double-logarithmic scale (Figure 2a). In our study, we could thereby estimate the number of HiBiT-FZD$_7$ molecules present on the surface of a single cell (Figure 2b). According to our calculations, a single HiBiT-FZD$_7$ SW480 cell expresses on average 1373 ± 349 FZD$_7$ proteins on its surface. Similarly, we applied these calculations to measurements on overexpressing and highly overexpressing HiBiT-FZD$_7$ SW480 cells (Figure 2b), which resulted in average values of 7034 ± 806 and 42,609 ± 2383 membrane receptors per cell, respectively. These estimations show that overexpression results in ~5-fold and high overexpression results in ~31-fold increase of HiBiT-FZD$_7$ number in these cells. Next, we analysed the total expression of HiBiT-FZD$_7$ and aimed to assess the fraction of intracellular HiBiT-FZD$_7$ molecules, which are not accessible for LgBiT at the time of measurement in the live-cell setup. To this end, we measured NanoBiT-associated luminescence after treating the cells with 100 µg·ml^{-1} (0.01%) digitonin for 10 min (B. L. Hoare et al., 2019). It is important to note that digitonin selectively permeabilizes the plasma membrane but leaves other organelles, such as endoplasmic reticulum, intact (Plutner et al., 1992). Importantly, a stronger detergent Triton X-100 could not be used in this setup as it has been reported to quench Nluc luminescence (Hoare et al., 2019). First, we could demonstrate that all detectable endogenous HiBiT-FZD$_7$ proteins are localized at the cell membrane, when no additional receptors have been introduced by transient transfection (Figure S3a), as there was no increase in luminescence upon pre-treatment with digitonin. Second, the fraction of fully mature receptors not exposed at the cell surface increases with the increase in plasmid amount used in transfection and can account for 16–35% up to 65% of the cell-membranous pool (for luminescence counts = approximately 100,000 and 400,000 a.u., respectively; Figure S3B). The data can be fitted to a simple linear regression model ($R^2 = 0.84$; not significant deviation from linearity).

3.3 | Kinetic binding of eGFP-Wnt-3a to endogenous and overexpressed HiBiT-FZD$_7$

HiBiT-FZD$_7$ SW480 cells were used to study the binding kinetics of eGFP-Wnt-3a to endogenous FZD$_7$ and to FZD$_7$ overexpressed at two different expression levels. For these experiments, cells were first incubated with the complementary LgBiT protein and the long-lasting luciferase substrate endurazine. eGFP-Wnt-3a was added to final concentrations of 0.9, 1.8 or 2.7 nM and BRET readings were recorded over a 5-h period at 37°C (Figure 3). The kinetic analysis showed that eGFP-Wnt-3a associates to endogenously expressed HiBiT-FZD$_7$ in a saturable manner, reaching a plateau after approximately 80 min. However, in the case of receptor overexpression and even more so for high overexpression, the eGFP-Wnt-3a binding to HiBiT-FZD$_7$ occurred with a substantially slower on-rate (k_{on}) to reach only nearly saturable levels after the 5 h of experimental duration (Figure 3 and Table 1). On the contrary and as expected, the off-rate k_{off} (and the corresponding $t_{1/2}$) did not depend on the receptor expression levels.

3.4 | eGFP-Wnt-3a saturation binding to endogenous and overexpressed HiBiT-FZD$_7$

To define the equilibrium binding affinity (used interchangeably with K_d throughout) of eGFP-Wnt-3a in saturation binding experiments, we incubated HiBiT-FZD$_7$ SW480 cells (corresponding receptor expression presented in Figure 2b) with a full concentration range (0.027–9.0 nM) of eGFP-Wnt-3a (Figure 4). The net BRET ratio representing ligand–receptor binding increased in a clear concentration-dependent manner and reached saturation for HiBiT-FZD$_7$ SW480 cells expressing HiBiT-FZD$_7$ at endogenous and overexpression levels (Figure 4 top left and top right). On the contrary, eGFP-Wnt-3a binding to highly overexpressed HiBiT-FZD$_7$ did not saturate at the concentrations used and had itself a much lower apparent affinity (Figure 4 bottom). The apparent affinities of eGFP-Wnt-3a to HiBiT-FZD$_7$ were determined using a one-site specific non-linear regression model and the K_d values are shown in Table 1. We have used the data from individual experiments underlying the results presented in Figures 2b and 4 to display the correlation between HiBiT-FZD$_7$ expression levels and eGFP-Wnt-3a/FZD$_7$ binding affinities (Figure 5).

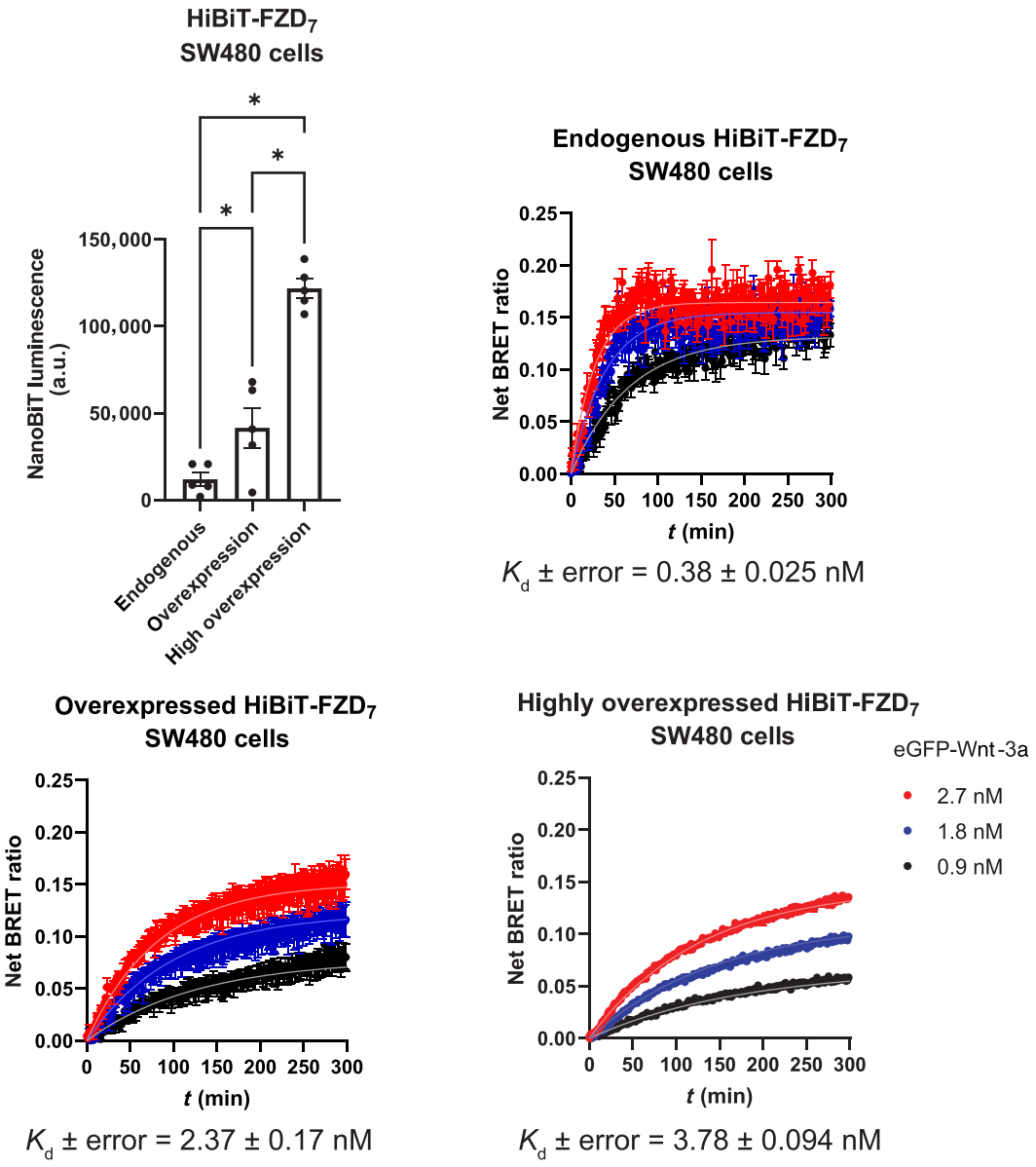

FIGURE 3 eGFP-Wnt-3a binding kinetics. Association kinetics of eGFP-Wnt-3a to HiBiT-FZD$_7$ expressed at the three different expression levels (endurazine was used as a substrate) were determined using 0.9, 1.8 and 2.7 nM of eGFP-Wnt-3a by detection of NanoBiT/BRET in living CRISPR-Cas9 genome-edited HiBiT-FZD$_7$ SW480 cells. NanoBiT/BRET was sampled once every 87 s for 300 min. Raw data were fitted to the 'two or more hot concentrations model' and are presented as mean ± SEM from n = 5 individual experiments. Kinetic parameters are summarized in Table 1. eGFP-Wnt-3a Batch 2 was used. *$P \leq 0.05$.

TABLE 1 Kinetic binding and saturation binding parameters of eGFP-Wnt-3a binding to HiBiT-FZD$_7$.

Kinetic binding parameters					Saturation binding
	K_d ± error (M^{-9})	k_{on} ± SEM ($M^{-1}\cdot min^{-1}$)	k_{off} ± SEM (min^{-1})	$t_{1/2}$ ± SEM (min)	K_d (95% CI) (M^{-9})
HiBiT-FZD$_7$ endogenous	0.38 ± 0.025	1.17 * 10^7 ± 0.025 * 10^7	0.0044 ± 0.0003	157.50 ± 10.05	1.98 (1.33–2.99)
HiBiT-FZD$_7$ overexpressed	2.37 ± 0.170	2.40 * 10^6 ± 0.11 * 10^6	0.0057 ± 0.0003	121.58 ± 6.08	4.48 (3.61–5.63)
HiBiT-FZD$_7$ highly overexpressed	3.78 ± 0.094	1.21 * 10^6 ± 0.024 * 10^6	0.0046 ± 0.0001	150.65 ± 3.20	20.75 (12.93–41.51)

Note: Values are based on data from n = 5 individual experiments (shown in Figures 3 and 4) and presented as a best fit value ± SEM.
Abbreviations: CI, confidence interval; FZD, Frizzleds.

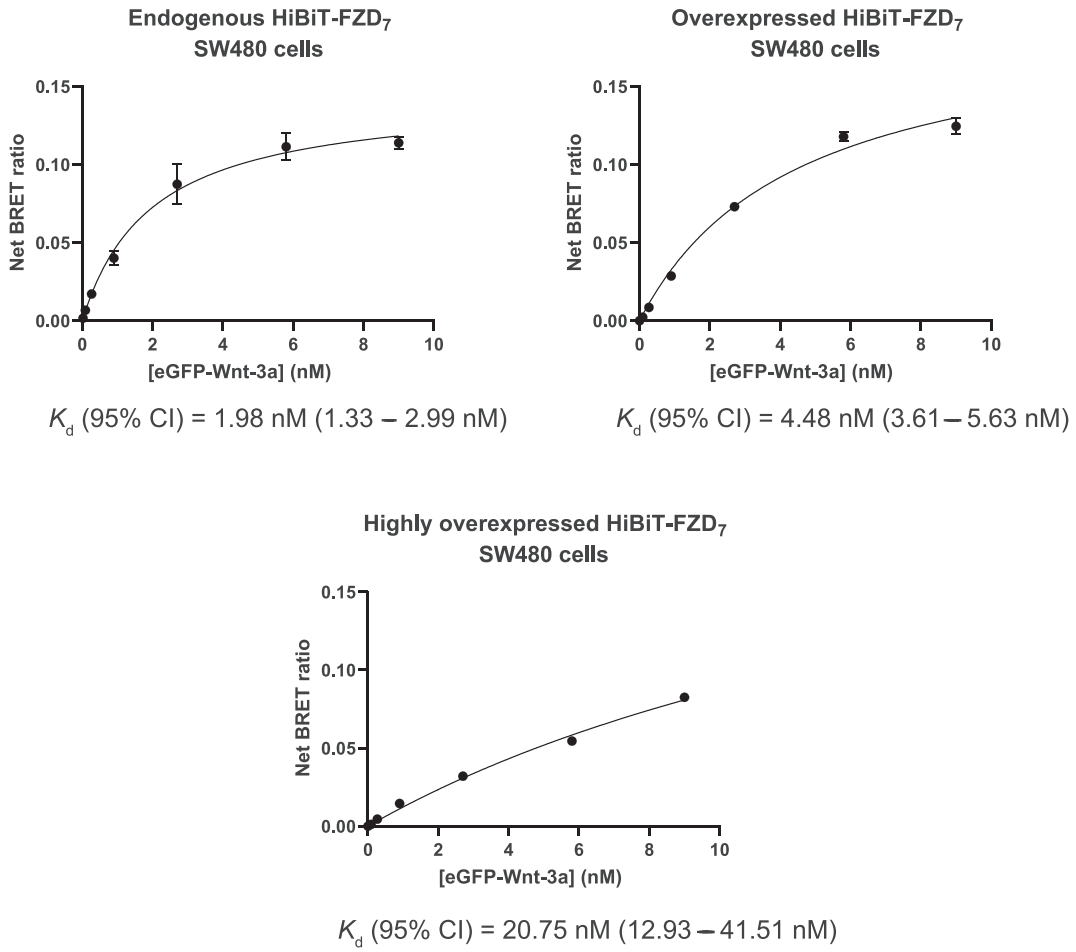

FIGURE 4 eGFP-Wnt-3a saturation binding. Saturation binding of the eGFP-Wnt-3a to HiBiT-FZD$_7$ expressed at the three different levels (presented in Figures 2b and S4B) in living CRISPR-Cas9 genome-edited HiBiT-FZD$_7$ SW480 cells was determined using a full concentrations range (0.027–9 nM) following 300 min of incubation. Raw data are presented as mean ± SEM from n = 5 individual experiments, fitting a one-site specific model. The equilibrium dissociation constants (K_d) are also summarized in Table 1. eGFP-Wnt-3a Batch 2 was used.

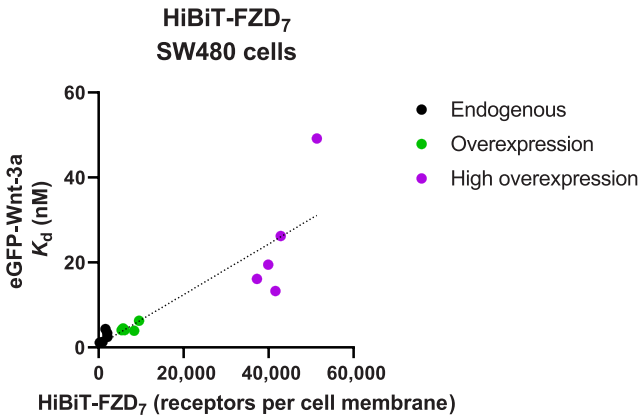

FIGURE 5 Correlation between eGFP-Wnt-3a apparent binding affinity measured with NanoBiT/BRET and number of HiBiT-FZD$_7$ molecules. The graphs present a correlation between eGFP-Wnt-3a K_d in nM (y-axis) and HiBiT-FZD$_7$ expression in molecules per cell membrane. Data points represent K_d and receptor molecule numbers come from each of n = 5 individual experiments for each condition (15 data points in total). The dotted line represents a simple linear regression fit.

These data could be fitted to a simple linear regression model ($R^2 = 0.77$; not significant deviation from linearity) arguing for a strong correlation between the measured apparent K_d values and receptor expression levels.

3.5 | Wnt-3a-induced HiBiT-FZD$_7$ internalization, total HiBiT-FZD$_7$ expression and their effect on ligand binding measurements

As eGFP-Wnt-3a is a FZD$_7$ agonist, we aimed to determine the effects of a potential Wnt-3a-induced HiBiT-FZD$_7$ internalization on the assessment of ligand affinity by measuring NanoBiT-emitted luminescence following the stimulation of HiBiT-FZD$_7$ SW480 cells with Wnt-3a. We used a recombinant untagged, high-purity, human Wnt-3a at a concentration of 9.0 nM, matching the highest fluorescent ligand concentration used in the ligand binding assays described above. For the cells expressing HiBiT-FZD$_7$ at endogenous levels, incubation with a fixed Wnt-3a concentration led to a time-

dependent decrease in luminescence emitted by NanoBiT followed by a plateau (Figure 6a). On the contrary, for overexpressing and highly overexpressing cells, Wnt-3a led to a visibly faster but proportionally less prominent reduction in cell-membrane-associated HiBiT-FZD$_7$ luminescence, which was followed by its rise to baseline (Figure 6a top). Likewise, NanoBiT/BRET kinetic binding curves with eGFP-Wnt-3a used at 9.0 nM also showed distinct profiles for endogenous and overexpressed receptors (Figure 6a bottom). These results point

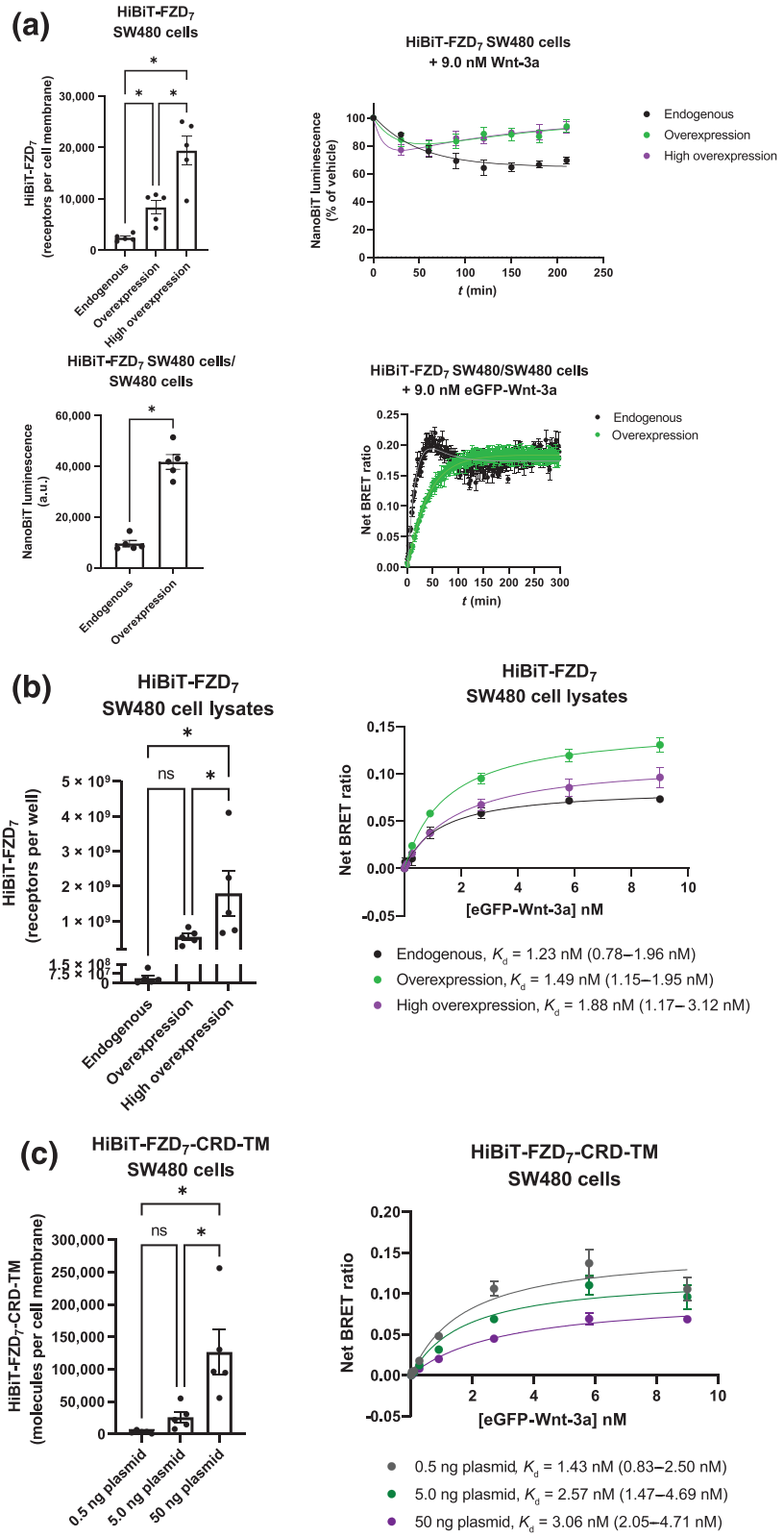

FIGURE 6 Impact of Wnt-3a-induced internalization of HiBiT-FZD$_7$ on the NanoBiT/BRET ligand binding measurements. (a) (the top panel) The panel shows time courses of recombinant untagged high-purity human Wnt-3a-induced internalization of endogenous, overexpressed and highly overexpressed HiBiT-FZD$_7$ in HiBiT-FZD$_7$ SW480 cells (the expression data are on the left panel). Luminescence of cell surface complemented HiBiT–LgBiT (NanoBiT) was measured after 210 min following additions of 9 nM of Wnt-3a in 30 min of intervals (the right panel). Normalized data are presented as mean ± SEM from n = 5 individual experiments and fitted to a fall to steady state time course (endogenous HiBiT-FZD$_7$ expression) or fall-and-rise to baseline (HiBiT-FZD$_7$ overexpression and high overexpression) equations. (the bottom panel) Association kinetics of eGFP-Wnt-3a to HiBiT-FZD$_7$ expressed at the two different expression levels were determined using 9.0 nM of eGFP-Wnt-3a by detection of NanoBiT/BRET in living HiBiT-FZD$_7$ SW480 cells (endogenous) or SW480 cells (overexpression). NanoBiT/BRET was sampled once every 87 s for 180 min. Raw data were fitted to the one-phase association model (overexpressed) or rise-and-fall to steady state (endogenous) and are presented as mean ± SEM from n = 5 individual experiments. eGFP-Wnt-3a Batch 2 was used. (b) Saturation binding of the eGFP-Wnt-3a to endogenous, overexpressed and highly overexpressed HiBiT-FZD$_7$ (the expression data on the left panel) in whole-cell lysates of CRISPR-Cas9 genome-edited HiBiT-FZD$_7$ SW480 was determined using a full concentrations range (0.027–9 nM) following 300 min of incubation (the right panel). Raw data are presented as mean ± SEM from n = 5 individual experiments, fitting a one-site specific model. eGFP-Wnt-3a Batch 3 was used. There is a significant difference in HiBiT-FZD$_7$ expression between endogenous and overexpressed conditions when they are compared with paired *t*-test ($P = 0.004$). (c) Saturation binding of the eGFP-Wnt-3a to HiBiT-FZD$_7$-CRD-TM overexpressed at three different levels (the left panel) in SW480 cells was determined using a full concentrations range (0.027–9 nM) following 300 min of incubation (the right panel). Amount of transfected plasmid DNA is presented as per well of a 96-well plate. Raw data are presented as mean ± SEM from n = 5 individual experiments, fitting a one-site specific model. eGFP-Wnt-3a Batch 3 was used. There is a significant difference in HiBiT-FZD$_7$-CRD-TM expression between endogenous and overexpressed conditions when they are compared with Student's unpaired *t*-test ($P = 0.024$). *$P \leq 0.05$.

towards differences in HiBiT-FZD_7 turnover in cell membranes for various expression levels in live SW480 cells. Next, we measured the impact of the cell-membranous receptor internalization and turnover on the ligand binding affinity measurements. To this end, we used HiBiT-FZD_7 SW480 cell lysates where cell membrane integrity is compromised, intracellular components are released and the aforementioned internalization and turnover are not feasible. We incubated the lysates with increasing concentrations of eGFP-Wnt-3a. We employed the same setup as in the saturation binding experiments on live cells. As opposed to the live-cell setup, we detected a concentration-dependent saturable binding of eGFP-Wnt-3a to HiBiT-FZD_7 for all three expression levels (Figure 6b). The ligand binding presented itself with non-significantly different K_d (95% CI) values of 1.23 nM (0.78–1.96 nM), 1.49 nM (1.15–1.95 nM) and 1.88 nM (1.17–3.12 nM) for endogenous, overexpressed and highly overexpressed conditions, respectively. In a set of complementary experiments to further address the impact of internalization on the ligand binding, we employed a membrane-anchored FZD_7 CRD (HiBiT-FZD_7-CRD-TM) and analysed eGFP-Wnt-3a binding to this isolated and less dynamic representation of the Wnt-3a binding site. We could show that eGFP-Wnt-3a bound the CRD with the same K_d irrespective of the number of binding sites present at the cell surface (K_d [95% CI] 1.43 nM [0.83–2.50 nM], 2.57 nM [1.47–4.69 nM] and 3.06 nM [2.05–4.71 nM] for the 0.5 ng [3316 ± 986 binding sites], 5.0 ng [25,919 ± 8161 binding sites] and 50 ng [126,606 ± 34,491 binding sites] of HiBiT-FZD_7-CRD-TM plasmid DNA per well, respectively; Figure 6c).

4 | DISCUSSION AND CONCLUSIONS

Here, we have developed a NanoBiT/BRET system to analyse eGFP-Wnt-3a binding to HiBiT-FZD_7 expressed from its endogenous promotor in SW480 cells typifying colorectal cancer. Additionally, we have used our newly generated cells to estimate the number of FZD_7 molecules on the surface of these cells and assessed Wnt-3a-induced internalization and turnover of HiBiT-FZD_7 by measuring NanoBiT-emitted luminescence at endogenous levels and upon receptor overexpression. Importantly, this is the first study to quantify Wnt binding to a tagged, full-length FZD expressed from its endogenous promoter. Moreover, it has to be noted that there have only been two studies on Wnt–FZD BRET binding so far (Kozielewicz et al., 2021; Wesslowski et al., 2020) and, thus, we are mostly limited to discussing our previous findings or linking our results to the data from Class A GPCRs (White et al., 2020).

We performed the experiments in a SW480 colorectal cancer model to provide a more relevant system to study Wnt–FZD biology than the commonly used HEK293 cells, which also provided an opportunity to compare Wnt binding to overexpressed FZDs with binding to FZDs expressed at lower, endogenous numbers (Kozielewicz et al., 2021). A recent study demonstrated that reducing the expression of the Wnt co-receptor LRP6 to endogenous levels resulted in an increase in ligand binding affinity of their ligands, DKK proteins (Eckert et al., 2020). Here, we used CRISPR-Cas9 genome editing in SW480 cells to insert an 11-amino-acid HiBiT tag to the 5′ end of the endogenous FZD_7 locus. We have previously demonstrated that the addition of a HiBiT tag does not compromise the receptor's functions, as recombinant overexpressed human HiBiT-FZD_7 was capable of binding eGFP-Wnt-3a and mediating Wnt-3a-induced β-catenin-dependent signalling (Kozielewicz et al., 2021). It has to be noted that the addition of the tag was the only genome edition of the FZD_7 gene we performed here as we have kept the native FZD_7 signal peptide and we have not introduced any silent mutations or restriction sites. Here, it should be mentioned that SW480 cells are defined as hyperdiploid (Kleivi et al., 2004). As such, non-diploid cells have posed difficulties in establishing homozygous clones following genome editing with CRISPR-Cas9 (White et al., 2019). Hence, to analyse the efficiency of CRISPR-Cas9 tagging and to prove the homozygotic status of the clones, we performed Sanger sequencing. Sequencing of the FZD_7-specific PCR product amplified from genomic DNA resulted in a single distinct peak, indicating that we indeed generated a homozygous clonal line. These results were then further supported by sequencing of an 829-bp product from the mRNA template where again only a single sequencing signal was visible indicative of translation of one FZD_7 variant—HiBiT-FZD_7. Finally, the correct size and proper cell-surface trafficking of this membrane receptor have been confirmed with immunoblotting using anti-HiBiT antibody and NanoBiT-emitted luminescence, respectively. In summary, our analysis validated the generation of the engineered homozygous SW480 cell system.

Next, we have used our CRISPR-Cas9-edited cells to estimate the number of FZD_7 molecules on the cell surface using NanoBiT-emitted luminescence and HiBiT–LgBiT calibration curve. A similar approach has been presented previously to quantify expression of CXCL12-HiBiT in genome-edited HEK293 cells. Here, we assume that LgBiT has comparable affinity to the N-terminally HiBiT-tagged apo FZD_7 and to the purified HiBiT, as it has been shown that alterations in HiBiT–LgBiT complementation affinity could exist due to conformational changes in the tagged protein (White et al., 2020). Second, it should be noted that estimation of receptor numbers is based on the assumption that receptors are evenly expressed among the cells, which leads to underestimation of the total membrane-associated receptors number on a cell in the overexpressing paradigms (Figure S4A). We have performed assays in three experimental setups in the HiBiT-FZD_7 SW480 cells, using, (1) untransfected, (2) FZD_7-overexpressing or (3), FZD_7-highly overexpressing cells. The number of HiBiT-FZD_7 expressed on the cell surface of the live cells used in the saturation binding assays has increased ~5-fold following transfection of the cells with HiBiT-FZD_7 plasmid (10 ng of receptor plasmid DNA in a well). In the case of the high overexpression setup (100 ng of receptor plasmid DNA in a well), the number of FZD_7 was even boosted as much as 31 times. Importantly, overexpression of HiBiT-FZD_7 led to a significant proportion of receptors being expressed intracellularly in addition to the cell membrane pool, as demonstrated by the data with digitonin permeabilization (Figure S3). For the endogenous system, however, we observed that all mature FZD_7 molecules are indeed cell membrane bound.

Subsequently, we measured eGFP-Wnt-3a binding to HiBiT-FZD_7. First, we performed NanoBiT/BRET binding in a kinetic format. We monitored the association of the fluorescently tagged Wnt to HiBiT-tagged FZD_7 over a 5-h time period sampling BRET. We have detected clear receptor expression-dependent changes in the association rate constant k_{on}. To this end, eGFP-Wnt-3a binding to endogenous HiBiT-FZD_7 saturated after approximately 80 min of incubation for two of three employed ligand concentrations. On the contrary, the association to the overexpressed and highly overexpressed receptors presented itself with curves, which did not reach full saturation during the experiment time. Thus, we observed changes in the kinetic binding parameters with particularly dramatic differences in the association rate constants (k_{on}) leading to differences in kinetic K_d values. At the same time, the dissociation rate constants (k_{off}) were not correlated to receptor expression levels and generally slow for the three conditions arguing for an equally long action of the FZD_7 ligand. Wnt proteins are highly lipophilic and we hypothesize that the slow off-rate could be explained by the fact that Wnts are not readily dispersed in an aqueous solution. Likewise, slow off-rates have been reported previously for Wnt-3a binding to a soluble FZD_7 CRD (Dijksterhuis et al., 2015). It has to be appreciated that even though the luminescence values for endogenously expressing cells were close to the lower detection limit of the plate reader (Figure S4B) and not detectable by fluorescent staining with confocal microscopy (Figure S4A), we were still able to detect eGFP-Wnt-3a binding to HiBiT-FZD_7 in a robust manner. We also performed saturation binding studies, in which we incubated the HiBiT-FZD_7 cells with the fluorescent ligand. Here, we incubated eGFP-Wnt-3a with the cells for 5 h to subsequently report apparent binding affinities that are likely underestimates of true binding affinities reported in the kinetic binding study. With this caveat, the data still support the notion that higher receptor expression levels of HiBiT-FZD_7 lead to a lower apparent measured binding affinity (higher apparent K_d in nM) of eGFP-Wnt-3a. Importantly, the apparent measured binding affinities of eGFP-Wnt-3a to highly overexpressed HiBiT-FZD_7 in SW480 cells were comparable with those we have obtained in HEK293A cells under similar experimental conditions (Kozielewicz et al., 2021).

In classical radioligand binding assays using cell membranes or whole-cell lysates, an increase in receptor expression could lead to ligand depletion due to the receptor binding, partition of the tracer into cell membranes and other non-specific interactions (C. A. Flanagan, 2016). To prevent this, the receptor concentration should generally not exceed a 10th of the K_d value of the used tracer molecule (Hulme & Trevethick, 2010). As such, selective targeting of membrane receptors in the NanoBiT/BRET setup greatly limits any impact of non-specific interactions and compartmentalization that cannot interfere with the BRET readout due to the far distance from the NanoBiT-tagged receptor at which they occur. We also followed effective equilibration times for high affinity ligands (Hoare, 2021) and our data were initially also not explainable by ligand depletion (Figure S5). In these calculations, we used the data from the saturation binding experiments, where the receptor concentrations ± SEM were equal to 1.65 ± 0.42, 8.47 ± 0.97 and 51.30 ± 2.87 pM for the endogenous, overexpressed and highly overexpressed conditions, respectively (data from Figure 2). However, we show that HiBiT-FZD_7 overexpression leads to a significant fraction of the receptors present in other compartments than the cell membrane alone. Moreover, Wnt-3a-induced HiBiT-FZD_7 internalization displays different kinetics profiles between endogenous and overexpressed/highly overexpressed receptors. In these experiments, a decrease in luminescence was indicative of a reduction in the number of the membrane-localized receptors. To this end, the membranous pool of overexpressed and highly overexpressed HiBiT-FZD_7 was replenished already within 3.5 h of the ligand internalization experiment. On the contrary, for the endogenous receptors, we observed a slower and gradual decrease in the luminescence signal that reached a plateau without returning to the baseline. These results suggest that overexpressed FZD_7 presents with a more dynamic membrane expression profile in comparison with endogenously expressed receptors. Our observations are supported by published data from reports on trafficking and signalling of this FZD paralogue, internalization studies with FZD_7-specific antibody fragment in human embryonic stem cell and analyses performed in Wilms' tumour (Egea-Jimenez et al., 2016; Fernandez et al., 2014; Pode-Shakked et al., 2011). Similarly, impact of agonist-induced receptor endocytosis on NanoBRET ligand binding has been noted for **neurotensin receptor type 1 (NTS_1) receptor**, **angiotensin II type 1 (AT_1) receptor** and **vascular endothelial growth factor 2 receptor 2 (VEGFR-2)** (Gratz et al., 2022; Kilpatrick et al., 2017; Peach et al., 2019). Thus, it is likely that discrepancies between measured ligand affinities in our systems are due to the combined effects of altered ligand–receptor internalization and substantial membrane turnover of HiBiT-FZD_7 in overexpressed and highly overexpressed conditions. We suspect that, for the transiently transfected systems, there would be a decrease in true ligand concentration after 5 h in comparison with the initial concentration, with the average number of cell-membranous receptors being similar to the initial number due to their recycling. Moreover, this receptor recycling is likely also the reason for the slow observed k_{on} in the kinetic binding studies with overexpressed and highly overexpressed receptors where a steady replenishment of cell surface receptors would prevent ligand binding saturation. Our hypotheses are further strengthened by the data from the saturation binding experiments with whole-cell lysates and with the membrane-anchored HiBiT-FZD_7 CRD (Figure 6). In these assays, we reported no significant differences in K_d values between the three receptor expression levels and the three different binding site expression levels. Lastly, it has to be noted that the aforementioned calculations (Hoare, 2021) do not take this receptors dynamics, specifically trafficking, in live cells into account.

Finally, we attempted to assess if eGFP-Wnt-3a binding to HiBiT-FZD_7 can be modified by other biological processes. As such, modulation of DKK1–eGFP binding affinity to Wnt receptor LRP6 has been linked to a potential role of receptor–receptor interactions that become more prevalent following receptor overexpression (Eckert et al., 2020). To this end, differences in ligand binding affinities to monomeric and dimeric target proteins have been reported in the literature (Bessman et al., 2014; Boni-Schnetzler & Pilch, 1987). Along

these lines, FZD_7 can form homodimers upon overexpression (Felce et al., 2017). Here, we mathematically tested for any contribution of FZD_7 dimerization to ligand binding affinity and investigated the possibility of a more complex ligand binding scenario involving receptor dimers (C. White & Bridge, 2019). We noted that the dimerized receptors model fits the data and the one-site fit model for all three conditions. Thus, receptor dimerization at least provides a plausible alternative model for Wnt-3a/FZD_7 binding, in addition to the one-site model. Of note, the pre-dimerized model predicted a negative equilibrium cooperativity; that is, the ligand has lower affinity for the second protomer when the first protomer is bound by the ligand (Figure S6). Next, we assessed the contribution of eGFP-Wnt-3a interaction with LRP5/6 to the observed ligand affinity for HiBiT-FZD_7 as Wnt-3a binds both FZD_7 and LRP6 to initiate β-catenin-dependent signalling (Nile et al., 2018). We used the saturation binding setup to measure eGFP-Wnt-3a association with endogenous HiBiT-FZD_7 in the presence of 11.6 nM (300 ng·ml^{-1}) of unlabelled recombinant human DKK1 (Figure S7), which blocks the Wnt-3a binding sites on LRP5/6 (https://www.rndsystems.com/products/recombinant-human-dkk-1-protein_5439-dk). In this way, we created conditions where available HiBiT-FZD_7 binding sites for eGFP-Wnt-3a likely outnumbered available LRP5/6 binding sites. However, in these saturation binding experiments, we did not detect a difference in the K_d of eGFP-Wnt-3a to endogenous HiBiT-FZD_7 in the presence of DKK1 compared with the results presented in Table 1 (K_d with DKK1 [95% CI] = 2.42 nM [1.91–3.09 nM]). These data indicate that LRP5/6 binding does not contribute to the Wnt affinity to HiBiT-FZD_7 expressed in a native cell context.

In summary, we report on the development of a novel NanoBiT/BRET binding assay that allows analysis of ligand binding to endogenous FZD_7. Our results suggest that studying eGFP-Wnt-3a binding to HiBiT-FZD_7 using endogenously expressed receptors is superior to employing overexpressed conditions. When overexpressed at different levels, HiBiT-FZD_7 has a very dynamic membrane profile that leads to seemingly incorrect measurements of ligand–receptor interactions. Thus, this study, applicable so far only to Wnt-3a and FZD_7, provides a plausible explanation for the requirement of high concentrations of Wnt-3a for the FZD_7-cpGFP conformation sensor readout in the HEK293 overexpression system (Schihada et al., 2020). With the development of other fluorescent Wnts, FZD-binding small molecules and the generation of relevant cell lines expressing low levels of other FZD paralogues, our concepts and tools can be used to more accurately compare and profile Wnt–FZD binding selectivity and optimize drug development campaigns to establish FZD-targeting anticancer drugs.

AUTHOR CONTRIBUTIONS

Lukas Grätz: Conceptualization (equal); data curation (equal); formal analysis (equal); funding acquisition (supporting); investigation (equal); methodology (equal); resources (supporting); validation (equal); visualization (equal); writing—original draft (equal); writing—review and editing (equal). **Joanna J. Sajkowska-Kozielewicz:** Data curation (supporting); formal analysis (supporting); investigation (equal); methodology (equal); resources (supporting); validation (supporting); visualization (equal); writing—original draft (supporting); writing—review and editing (supporting). **Janine Wesslowski:** Data curation (supporting); formal analysis (supporting); investigation (supporting); methodology (supporting); resources (supporting); validation (supporting); visualization (supporting). **Julia Kinsolving:** Data curation (supporting); resources (supporting); writing—review and editing (supporting). **Lloyd J. Bridge:** Formal analysis (supporting); methodology (supporting); visualization (supporting); writing—review and editing (supporting). **Katja Petzold:** Funding acquisition (supporting); project administration (supporting); resources (supporting); supervision (supporting); writing—original draft (supporting); writing—review and editing (supporting). **Gary Davidson:** Conceptualization (supporting); funding acquisition (supporting); project administration (supporting); resources (supporting); supervision (supporting); writing—original draft (supporting); writing—review and editing (supporting). **Gunnar Schulte:** Conceptualization (equal); funding acquisition (lead); project administration (equal); resources (equal); supervision (equal); validation (equal); writing—original draft (equal); writing—review and editing (equal). **Paweł Kozielewicz:** Conceptualization (lead); data curation (equal); formal analysis (equal); funding acquisition (equal); investigation (lead); methodology (lead); project administration (equal); resources (equal); supervision (equal); validation (equal); visualization (lead); writing—original draft (lead); writing—review and editing (lead).

ACKNOWLEDGEMENTS

This study was supported by the Karolinska Institute, the Swedish Cancer Society (Cancerfonden) (CAN2018/715, 20 0264P, 20 1102 PjF), the Swedish Research Council (Vetenskapsrådet) (2019-01190), the Knut and Alice Wallenberg Foundation (Knut och Alice Wallenbergs Stiftelse) (2016.0087), the Novo Nordisk Foundation (Novo Nordisk Fonden) (NNF22OC0078104, NNF21OC00700, NNF20OC0063168), the Lars Hierta Memorial Foundation (Stiftelsen Lars Hiertas Minne) (FO2020-0304, FO2021-0127) and the German Research Foundation (Deutsche Forschungsgemeinschaft) (504098926 and 331351713-SFB 1324; project A06 to G. D.).

CONFLICT OF INTEREST STATEMENT

The authors declare no conflicts of interest.

DATA AVAILABILITY STATEMENT

The data that support the findings of this study are available from the corresponding author upon reasonable request.

DECLARATION OF TRANSPARENCY AND SCIENTIFIC RIGOUR

This Declaration acknowledges that this paper adheres to the principles for transparent reporting and scientific rigour of preclinical research as stated in the *BJP* guidelines for Design and Analysis and Immunoblotting and Immunochemistry, and as recommended by funding agencies, publishers and other organizations engaged with supporting research.

ORCID

Lukas Grätz https://orcid.org/0000-0001-6755-0742

Joanna J. Sajkowska-Kozielewicz https://orcid.org/0000-0003-1140-2753

Janine Wesslowski https://orcid.org/0000-0003-3674-1372

Julia Kinsolving https://orcid.org/0000-0002-0431-8222

Lloyd J. Bridge https://orcid.org/0000-0003-3289-788X

Katja Petzold https://orcid.org/0000-0001-9470-0347

Gary Davidson https://orcid.org/0000-0002-2264-5518

Gunnar Schulte https://orcid.org/0000-0002-2700-7013

Paweł Kozielewicz https://orcid.org/0000-0003-1414-3566

REFERENCES

Agostino, M., & Pohl, S. O. (2019). Wnt binding affinity prediction for putative Frizzled-type cysteine-rich domains. *International Journal of Molecular Sciences*, *20*(17), 4168. https://doi.org/10.3390/ijms20174168

Agostino, M., Pohl, S. O., & Dharmarajan, A. (2017). Structure-based prediction of Wnt binding affinities for Frizzled-type cysteine-rich domains. *The Journal of Biological Chemistry*, *292*(27), 11218–11229. https://doi.org/10.1074/jbc.M117.786269

Alexander, S. P. H., Christopoulos, A., Davenport, A. P., Kelly, E., Mathie, A., Peters, J. A., Veale, E. L., Armstrong, J. F., Faccenda, E., Harding, S. D., Pawson, A. J., Southan, C., Davies, J. A., Abbracchio, M. P., Alexander, W., Al-Hosaini, K., Bäck, M., Barnes, N. M., Bathgate, R., … Ye, R. D. (2021). The Concise Guide to PHARMACOLOGY 2021/22: G protein-coupled receptors. *British Journal of Pharmacology*, *178*, S27–S156. https://doi.org/10.1111/bph.15538

Alexander, S. P. H., Roberts, R. E., Broughton, B. R. S., Sobey, C. G., George, C. H., Stanford, S. C., Cirino, G., Docherty, J. R., Giembycz, M. A., Hoyer, D., Insel, P. A., Izzo, A. A., Ji, Y., MacEwan, D. J., Mangum, J., Wonnacott, S., & Ahluwalia, A. (2018). Goals and practicalities of immunoblotting and immunohistochemistry: A guide for submission to the *British Journal of Pharmacology*. *British Journal of Pharmacology*, *175*(3), 407–411. https://doi.org/10.1111/bph.14112

Bessman, N. J., Bagchi, A., Ferguson, K. M., & Lemmon, M. A. (2014). Complex relationship between ligand binding and dimerization in the epidermal growth factor receptor. *Cell Reports*, *9*(4), 1306–1317. https://doi.org/10.1016/j.celrep.2014.10.010

Bhanot, P., Brink, M., Samos, C. H., Hsieh, J. C., Wang, Y., Macke, J. P., Andrew, D., Nathans, J., & Nusse, R. (1996). A new member of the *frizzled* family from *Drosophila* functions as a Wingless receptor [Research Support, Non-U.S. Gov't Research Support, U.S. Gov't, Non-P.H.S.]. *Nature*, *382*(6588), 225–230. https://doi.org/10.1038/382225a0

Boni-Schnetzler, M., & Pilch, P. F. (1987). Mechanism of epidermal growth factor receptor autophosphorylation and high-affinity binding. *Proceedings of the National Academy of Sciences of the United States of America*, *84*(22), 7832–7836. https://doi.org/10.1073/pnas.84.22.7832

Burgy, O., & Konigshoff, M. (2018). The WNT signaling pathways in wound healing and fibrosis. *Matrix Biology*, *68-69*, 67–80. https://doi.org/10.1016/j.matbio.2018.03.017

Curtis, M. J., Alexander, S. P. H., Cirino, G., George, C. H., Kendall, D. A., Insel, P. A., Izzo, A. A., Ji, Y., Panettieri, R. A., Patel, H. H., Sobey, C. G., Stanford, S. C., Stanley, P., Stefanska, B., Stephens, G. J., Teixeira, M. M., Vergnolle, N., & Ahluwalia, A. (2022). Planning experiments: Updated guidance on experimental design and analysis and their reporting III. *British Journal of Pharmacology*, *179*, 3907–3913. https://doi.org/10.1111/bph.15868

Davidson, G. (2021). LRPs in WNT signalling. *Handbook of Experimental Pharmacology*, *269*, 45–73. https://doi.org/10.1007/164_2021_526

Deshpande, I., Liang, J., Hedeen, D., Roberts, K. J., Zhang, Y., Ha, B., Latorraca, N. R., Faust, B., Dror, R. O., Beachy, P. A., Myers, B. R., & Manglik, A. (2019). Smoothened stimulation by membrane sterols drives Hedgehog pathway activity. *Nature*, *571*(7764), 284–288. https://doi.org/10.1038/s41586-019-1355-4

Dijksterhuis, J. P., Baljinnyam, B., Stanger, K., Sercan, H. O., Ji, Y., Andres, O., Rubin, J. S., Hannoush, R. N., & Schulte, G. (2015). Systematic mapping of WNT-FZD protein interactions reveals functional selectivity by distinct WNT-FZD pairs. *The Journal of Biological Chemistry*, *290*(11), 6789–6798. https://doi.org/10.1074/jbc.M114.612648

Dixon, A. S., Schwinn, M. K., Hall, M. P., Zimmerman, K., Otto, P., Lubben, T. H., Butler, B. L., Binkowski, B. F., Machleidt, T., Kirkland, T. A., Wood, M. G., Eggers, C. T., Encell, L. P., & Wood, K. V. (2016). NanoLuc complementation reporter optimized for accurate measurement of protein interactions in cells. *ACS Chemical Biology*, *11*(2), 400–408. https://doi.org/10.1021/acschembio.5b00753

Do, M., Wu, C. C. N., Sonavane, P. R., Juarez, E. F., Adams, S. R., Ross, J., Baena, A. R. Y., Patel, C., Mesirov, J. P., Carson, D. A., Advani, S. J., & Willert, K. (2022). A FZD7-specific antibody-drug conjugate induces ovarian tumor regression in preclinical models. *Molecular Cancer Therapeutics*, *21*(1), 113–124. https://doi.org/10.1158/1535-7163.Mct-21-0548

Eckert, A. F., Gao, P., Wesslowski, J., Wang, X., Rath, J., Nienhaus, K., Davidson, G., & Nienhaus, G. U. (2020). Measuring ligand-cell surface receptor affinities with axial line-scanning fluorescence correlation spectroscopy. *eLife*, *9*, 1–29. https://doi.org/10.7554/eLife.55286

Egea-Jimenez, A. L., Gallardo, R., Garcia-Pino, A., Ivarsson, Y., Wawrzyniak, A. M., Kashyap, R., Loris, R., Schymkowitz, J., Rousseau, F., & Zimmermann, P. (2016). Frizzled 7 and PIP2 binding by syntenin PDZ2 domain supports Frizzled 7 trafficking and signalling. *Nature Communications*, *7*, 12101. https://doi.org/10.1038/ncomms12101

Felce, J. H., Latty, S. L., Knox, R. G., Mattick, S. R., Lui, Y., Lee, S. F., Klenerman, D., & Davis, S. J. (2017). Receptor quaternary organization explains G protein-coupled receptor family structure. *Cell Reports*, *20*(11), 2654–2665. https://doi.org/10.1016/j.celrep.2017.08.072

Fernandez, A., Huggins, I. J., Perna, L., Brafman, D., Lu, D., Yao, S., Gaasterland, T., Carson, D. A., & Willert, K. (2014). The WNT receptor FZD7 is required for maintenance of the pluripotent state in human embryonic stem cells. *Proceedings of the National Academy of Sciences of the United States of America*, *111*(4), 1409–1414. https://doi.org/10.1073/pnas.1323697111

Flanagan, C. A. (2016). GPCR-radioligand binding assays. *Methods in Cell Biology*, *132*, 191–215. https://doi.org/10.1016/bs.mcb.2015.11.004

Flanagan, D. J., Barker, N., Costanzo, N. S. D., Mason, E. A., Gurney, A., Meniel, V. S., Koushyar, S., Austin, C. R., Ernst, M., Pearson, H. B., Boussioutas, A., Clevers, H., Phesse, T. J., & Vincan, E. (2019). *Frizzled-7* is required for Wnt signaling in gastric tumors with and without *Apc* mutations. *Cancer Research*, *79*(5), 970–981. https://doi.org/10.1158/0008-5472.CAN-18-2095

Foord, S. M., Bonner, T. I., Neubig, R. R., Rosser, E. M., Pin, J. P., Davenport, A. P., Spedding, M., & Harmar, A. J. (2005). International Union of Pharmacology. XLVI. G protein-coupled receptor list [Review]. *Pharmacological Reviews*, *57*(2), 279–288. https://doi.org/10.1124/pr.57.2.5

Gibson, T. J., Seiler, M., & Veitia, R. A. (2013). The transience of transient overexpression. *Nature Methods*, *10*(8), 715–721. https://doi.org/10.1038/nmeth.2534

Gordon, M. D., & Nusse, R. (2006). Wnt signaling: Multiple pathways, multiple receptors, and multiple transcription factors [Review]. *The Journal of Biological Chemistry*, *281*(32), 22429–22433. https://doi.org/10.1074/jbc.R600015200

Goulding, J., Mistry, S. J., Soave, M., Woolard, J., Briddon, S. J., White, C. W., Kellam, B., & Hill, S. J. (2021). Subtype selective fluorescent ligands based on ICI 118,551 to study the human β2-adrenoceptor in CRISPR/Cas9 genome-edited HEK293T cells at low expression levels. *Pharmacology Research & Perspectives*, *9*(3), e00779. https://doi.org/10.1002/prp2.779

Gratz, L., Laasfeld, T., Allikalt, A., Gruber, C. G., Pegoli, A., Tahk, M. J., Tsernant, M. L., Keller, M., & Rinken, A. (2021). BRET- and fluorescence anisotropy-based assays for real-time monitoring of ligand binding to M2 muscarinic acetylcholine receptors. *Biochimica et Biophysica Acta: Molecular Cell Research*, *1868*(3), 118930. https://doi.org/10.1016/j.bbamcr.2020.118930

Gratz, L., Muller, C., Pegoli, A., Schindler, L., Bernhardt, G., & Littmann, T. (2022). Insertion of Nanoluc into the extracellular loops as a complementary method to establish BRET-based binding assays for GPCRs. *ACS Pharmacology & Translational Science*, *5*(11), 1142–1155. https://doi.org/10.1021/acsptsci.2c00162

Hoare, B. L., Kocan, M., Bruell, S., Scott, D. J., & Bathgate, R. A. D. (2019). Using the novel HiBiT tag to label cell surface relaxin receptors for BRET proximity analysis. *Pharmacology Research & Perspectives*, *7*(4), e00513. https://doi.org/10.1002/prp2.513

Hoare, S. R. J. (2021). The problems of applying classical pharmacology analysis to modern in vitro drug discovery assays: Slow binding kinetics and high target concentration. *SLAS Discovery*, *26*(7), 835–850. https://doi.org/10.1177/24725552211019653

Hoare, S. R. J., Tewson, P. H., Quinn, A. M., Hughes, T. E., & Bridge, L. J. (2020). Analyzing kinetic signaling data for G-protein-coupled receptors. *Scientific Reports*, *10*(1), 12263. https://doi.org/10.1038/s41598-020-67844-3

Hsieh, J. C., Rattner, A., Smallwood, P. M., & Nathans, J. (1999). Biochemical characterization of Wnt-Frizzled interactions using a soluble, biologically active vertebrate Wnt protein. *Proceedings of the National Academy of Sciences of the United States of America*, *96*(7), 3546–3551. https://doi.org/10.1073/pnas.96.7.3546

Hsu, P. D., Lander, E. S., & Zhang, F. (2014). Development and applications of CRISPR-Cas9 for genome engineering. *Cell*, *157*(6), 1262–1278. https://doi.org/10.1016/j.cell.2014.05.010

Hulme, E. C., & Trevethick, M. A. (2010). Ligand binding assays at equilibrium: Validation and interpretation. *British Journal of Pharmacology*, *161*(6), 1219–1237. https://doi.org/10.1111/j.1476-5381.2009.00604.x

Janda, C. Y., Waghray, D., Levin, A. M., Thomas, C., & Garcia, K. C. (2012). Structural basis of Wnt recognition by Frizzled [Research Support, N.I.H., Extramural Research Support, Non-U.S. Gov't]. *Science*, *337*(6090), 59–64. https://doi.org/10.1126/science.1222879

Jung, Y. S., & Park, J. I. (2020). Wnt signaling in cancer: Therapeutic targeting of Wnt signaling beyond beta-catenin and the destruction complex. *Experimental & Molecular Medicine*, *52*(2), 183–191. https://doi.org/10.1038/s12276-020-0380-6

Kilpatrick, L. E., Friedman-Ohana, R., Alcobia, D. C., Riching, K., Peach, C. J., Wheal, A. J., Briddon, S. J., Robers, M. B., Zimmerman, K., Machleidt, T., Wood, K. V., Woolard, J., & Hill, S. J. (2017). Real-time analysis of the binding of fluorescent $VEGF_{165}a$ to VEGFR2 in living cells: Effect of receptor tyrosine kinase inhibitors and fate of internalized agonist-receptor complexes. *Biochemical Pharmacology*, *136*, 62–75. https://doi.org/10.1016/j.bcp.2017.04.006

Kleivi, K., Teixeira, M. R., Eknaes, M., Diep, C. B., Jakobsen, K. S., Hamelin, R., & Lothe, R. A. (2004). Genome signatures of colon carcinoma cell lines. *Cancer Genetics and Cytogenetics*, *155*(2), 119–131. https://doi.org/10.1016/j.cancergencyto.2004.03.014

Kowalski-Jahn, M., Schihada, H., Turku, A., Huber, T., Sakmar, T. P., & Schulte, G. (2021). Frizzled BRET sensors based on bioorthogonal labeling of unnatural amino acids reveal WNT-induced dynamics of the cysteine-rich domain. *Science Advances*, *7*(46), eabj7917. https://doi.org/10.1126/sciadv.abj7917

Kozielewicz, P., Bowin, C. F., Turku, A., & Schulte, G. (2020). A NanoBRET-based binding assay for smoothened allows real-time analysis of ligand binding and distinction of two binding sites for BODIPY-cyclopamine. *Molecular Pharmacology*, *97*(1), 23–34. https://doi.org/10.1124/mol.119.118158

Kozielewicz, P., Shekhani, R., Moser, S., Bowin, C. F., Wesslowski, J., Davidson, G., & Schulte, G. (2021). Quantitative profiling of WNT-3A binding to all human Frizzled paralogues in HEK293 cells by NanoBiT/BRET assessments. *ACS Pharmacology & Translational Science*, *4*(3), 1235–1245. https://doi.org/10.1021/acsptsci.1c00084

Kozielewicz, P., Turku, A., Bowin, C. F., Petersen, J., Valnohova, J., Canizal, M. C. A., Ono, Y., Inoue, A., Hoffmann, C., & Schulte, G. (2020). Structural insight into small molecule action on Frizzleds. *Nature Communications*, *11*(1), 414. https://doi.org/10.1038/s41467-019-14149-3

Kozielewicz, P., Turku, A., & Schulte, G. (2020). Molecular pharmacology of class F receptor activation. *Molecular Pharmacology*, *97*(2), 62–71. https://doi.org/10.1124/mol.119.117986

Mori, Y., Yoshida, Y., Satoh, A., & Moriya, H. (2020). Development of an experimental method of systematically estimating protein expression limits in HEK293 cells. *Scientific Reports*, *10*(1), 4798. https://doi.org/10.1038/s41598-020-61646-3

Nile, A. H., de Sousa, E. M. F., Mukund, S., Piskol, R., Hansen, S., Zhou, L., Zhang, Y., Fu, Y., Gogol, E. B., Komuves, L. G., Modrusan, Z., Angers, S., Franke, Y., Koth, C., Fairbrother, W. J., Wang, W., de Sauvage, F. J., & Hannoush, R. N. (2018). A selective peptide inhibitor of Frizzled 7 receptors disrupts intestinal stem cells. *Nature Chemical Biology*, *14*(6), 582–590. https://doi.org/10.1038/s41589-018-0035-2

Nusse, R., & Clevers, H. (2017). Wnt/β-catenin signaling, disease, and emerging therapeutic modalities. *Cell*, *169*(6), 985–999. https://doi.org/10.1016/j.cell.2017.05.016

Peach, C. J., Kilpatrick, L. E., Woolard, J., & Hill, S. J. (2019). Comparison of the ligand binding properties of fluorescent VEGF-A isoforms to VEGFR2 in living cells and membrane preparations using NanoBRET. *British Journal of Pharmacology*, *176*, 3220–3235. https://doi.org/10.1111/bph.14755

Petersen, J., Wright, S. C., Rodriguez, D., Matricon, P., Lahav, N., Vromen, A., Friedler, A., Stromqvist, J., Wennmalm, S., Carlsson, J., & Schulte, G. (2017). Agonist-induced dimer dissociation as a macromolecular step in G protein-coupled receptor signaling. *Nature Communications*, *8*(1), 226. https://doi.org/10.1038/s41467-017-00253-9

Plutner, H., Davidson, H. W., Saraste, J., & Balch, W. E. (1992). Morphological analysis of protein transport from the ER to Golgi membranes in digitonin-permeabilized cells: Role of the P58 containing compartment. *The Journal of Cell Biology*, *119*(5), 1097–1116. https://doi.org/10.1083/jcb.119.5.1097

Pode-Shakked, N., Harari-Steinberg, O., Haberman-Ziv, Y., Rom-Gross, E., Bahar, S., Omer, D., Metsuyanim, S., Buzhor, E., Jacob-Hirsch, J., Goldstein, R. S., Mark-Danieli, M., & Dekel, B. (2011). Resistance or sensitivity of Wilms' tumor to anti-FZD7 antibody highlights the Wnt pathway as a possible therapeutic target. *Oncogene*, *30*(14), 1664–1680. https://doi.org/10.1038/onc.2010.549

Sato, A., Yamamoto, H., Sakane, H., Koyama, H., & Kikuchi, A. (2010). Wnt5a regulates distinct signalling pathways by binding to Frizzled2 [Research Support, Non-U.S. Gov't]. *The EMBO Journal*, *29*(1), 41–54. https://doi.org/10.1038/emboj.2009.322

Schihada, H., Kowalski-Jahn, M., Turku, A., & Schulte, G. (2020). Deconvolution of WNT-induced Frizzled conformational dynamics with fluorescent biosensors. *Biosensors and Bioelectronics*, *177*, 112948. https://doi.org/10.1016/j.bios.2020.112948

Schulte, G. (2010). International Union of Basic and Clinical Pharmacology. LXXX. The class Frizzled receptors [Research Support, Non-U.S. Gov't Review]. *Pharmacological Reviews*, *62*(4), 632–667. https://doi.org/10.1124/pr.110.002931

Schulte, G., & Kozielewicz, P. (2019). Structural insight into Class F receptors—What have we learnt regarding agonist-induced activation? *Basic & Clinical Pharmacology & Toxicology*, *126*(Suppl 6), 17–24. https://doi.org/10.1111/bcpt.13235

Schulte, G., & Wright, S. C. (2018). Frizzleds as GPCRs—More conventional than we thought! *Trends in Pharmacological Sciences*, *39*(9), 828–842. https://doi.org/10.1016/j.tips.2018.07.001

Soave, M., Kellam, B., Woolard, J., Briddon, S. J., & Hill, S. J. (2020). NanoBiT complementation to monitor agonist-induced adenosine A1 receptor internalization. *SLAS Discovery*, *25*(2), 186–194. https://doi.org/10.1177/2472555219880475

Soave, M., Stoddart, L. A., White, C. W., Kilpatrick, L. E., Goulding, J., Briddon, S. J., & Hill, S. J. (2021). Detection of genome-edited and endogenously expressed G protein-coupled receptors. *The FEBS Journal*, *288*(8), 2585–2601. https://doi.org/10.1111/febs.15729

Swain, R. K., Katoh, M., Medina, A., & Steinbeisser, H. (2005). *Xenopus frizzled-4S*, a splicing variant of *Xfz4* is a context-dependent activator and inhibitor of Wnt/β-catenin signaling. *Cell Communication and Signaling: CCS*, *3*, 12. https://doi.org/10.1186/1478-811X-3-12

Takada, R., Mii, Y., Krayukhina, E., Maruyama, Y., Mio, K., Sasaki, Y., Shinkawa, T., Pack, C. G., Sako, Y., Sato, C., Uchiyama, S., & Takada, S. (2018). Assembly of protein complexes restricts diffusion of Wnt3a proteins. *Communications Biology*, *1*, 165. https://doi.org/10.1038/s42003-018-0172-x

Tran, B. M., Flanagan, D. J., Phesse, T. J., & Vincan, E. (2021). Frizzled$_7$ activates β-catenin-dependent and β-catenin-independent Wnt signalling pathways during developmental morphogenesis: Implications for therapeutic targeting in colorectal cancer. *Handbook of Experimental Pharmacology*, *269*, 251–277. https://doi.org/10.1007/164_2021_524

Ueno, K., Hiura, M., Suehiro, Y., Hazama, S., Hirata, H., Oka, M., Imai, K., Dahiya, R., & Hinoda, Y. (2008). Frizzled-7 as a potential therapeutic target in colorectal cancer. *Neoplasia*, *10*(7), 697–705. http://www.ncbi.nlm.nih.gov/pubmed/18592008, https://doi.org/10.1593/neo.08320, https://www.ncbi.nlm.nih.gov/pmc/articles/PMC2435005/pdf/neo1007_0697.pdf

Vincan, E., Darcy, P. K., Farrelly, C. A., Faux, M. C., Brabletz, T., & Ramsay, R. G. (2007). Frizzled-7 dictates three-dimensional organization of colorectal cancer cell carcinoids. *Oncogene*, *26*(16), 2340–2352. https://doi.org/10.1038/sj.onc.1210026

Vincan, E., Darcy, P. K., Smyth, M. J., Thompson, E. W., Thomas, R. J., Phillips, W. A., & Ramsay, R. G. (2005). Frizzled-7 receptor ectodomain expression in a colon cancer cell line induces morphological change and attenuates tumor growth [Research Support, Non-U.S. Gov't]. *Differentiation*, *73*(4), 142–153. https://doi.org/10.1111/j.1432-0436.2005.00015.x

Wesslowski, J., Kozielewicz, P., Wang, X., Cui, H., Schihada, H., Kranz, D., Karuna, M. P., Levkin, P., Gross, J. C., Boutros, M., Schulte, G., & Davidson, G. (2020). eGFP-tagged Wnt-3a enables functional analysis of Wnt trafficking and signaling and kinetic assessment of Wnt binding to full-length Frizzled. *The Journal of Biological Chemistry*, *295*(26), 8759–8774. https://doi.org/10.1074/jbc.RA120.012892

White, C., & Bridge, L. J. (2019). Ligand binding dynamics for pre-dimerised G protein-coupled receptor homodimers: Linear models and analytical solutions. *Bulletin of Mathematical Biology*, *81*(9), 3542–3574. https://doi.org/10.1007/s11538-017-0387-x

White, C. W., Caspar, B., Vanyai, H. K., Pfleger, K. D. G., & Hill, S. J. (2020). CRISPR-mediated protein tagging with nanoluciferase to investigate native chemokine receptor function and conformational changes. *Cell Chemical Biology*, *27*(5), 499–510 e497. https://doi.org/10.1016/j.chembiol.2020.01.010

White, C. W., Johnstone, E. K. M., See, H. B., & Pfleger, K. D. G. (2019). NanoBRET ligand binding at a GPCR under endogenous promotion facilitated by CRISPR/Cas9 genome editing. *Cellular Signalling*, *54*, 27–34. https://doi.org/10.1016/j.cellsig.2018.11.018

White, C. W., Kilpatrick, L. E., Pfleger, K. D. G., & Hill, S. J. (2021). A nanoluciferase biosensor to investigate endogenous chemokine secretion and receptor binding. *iScience*, *24*(1), 102011. https://doi.org/10.1016/j.isci.2020.102011

White, C. W., Vanyai, H. K., See, H. B., Johnstone, E. K. M., & Pfleger, K. D. G. (2017). Using nanoBRET and CRISPR/Cas9 to monitor proximity to a genome-edited protein in real-time. *Scientific Reports*, *7*(1), 3187. https://doi.org/10.1038/s41598-017-03486-2

Willert, K., & Nusse, R. (2012). Wnt proteins [Research Support, N.I.H., Extramural Research Support, Non-U.S. Gov't Review]. *Cold Spring Harbor Perspectives in Biology*, *4*(9), a007864. https://doi.org/10.1101/cshperspect.a007864

Willert, K. H. (2008). Isolation and application of bioactive Wnt proteins. *Methods in Molecular Biology*, *468*Ref #580 of 1340 in FRIZZLED.ref, 17–29. https://doi.org/10.1007/978-1-59745-249-6_2

Wright, S. C., Canizal, M. C. A., Benkel, T., Simon, K., Le Gouill, C., Matricon, P., Namkung, Y., Lukasheva, V., Konig, G. M., Laporte, S. A., Carlsson, J., Kostenis, E., Bouvier, M., Schulte, G., & Hoffmann, C. (2018). FZD_5 is a $G\alpha_q$-coupled receptor that exhibits the functional hallmarks of prototypical GPCRs. *Science Signaling*, *11*(559), 1–14. https://doi.org/10.1126/scisignal.aar5536

Wu, C. H., & Nusse, R. (2002). Ligand receptor interactions in the Wnt signaling pathway in *Drosophila* [Research Support, Non-U.S. Gov't Research Support, U.S. Gov't, P.H.S.]. *Journal of Biological Chemistry*, *277*(44), 41762–41769. https://doi.org/10.1074/jbc.M207850200

Xu, L., Chen, B., Schihada, H., Wright, S. C., Turku, A., Wu, Y., Han, G. W., Kowalski-Jahn, M., Kozielewicz, P., Bowin, C. F., Zhang, X., Li, C., Bouvier, M., Schulte, G., & Xu, F. (2021). Cryo-EM structure of constitutively active human Frizzled 7 in complex with heterotrimeric Gs. *Cell Research*, *31*, 1311–1314. https://doi.org/10.1038/s41422-021-00525-6

SUPPORTING INFORMATION

Additional supporting information can be found online in the Supporting Information section at the end of this article.

How to cite this article: Grätz, L., Sajkowska-Kozielewicz, J. J., Wesslowski, J., Kinsolving, J., Bridge, L. J., Petzold, K., Davidson, G., Schulte, G., & Kozielewicz, P. (2023). NanoBiT- and NanoBiT/BRET-based assays allow the analysis of binding kinetics of Wnt-3a to endogenous Frizzled 7 in a colorectal cancer model. *British Journal of Pharmacology*, 1–17. https://doi.org/10.1111/bph.16090